AN ABSTRACT OF THE THESIS OF

Timothy E. Link for the degree of Master of Science in Geology presented on June 29, 1998. Title: Seasonal Snowcover Dynamics Beneath Boreal Forest Canopies.

Abstract approved:

Redacted for Privacy

Danny Marks and Julia A. Jones

The accurate simulation of snowpack deposition and ablation beneath forested areas is confounded by the fact that the vegetation canopy strongly affects the snow surface energy balance. The canopy alters the radiation balance of the snowcover, and reduces the wind speed at the snow surface. Data collected as part of the BOREAS experiment are used to analyze the effects of a variety of forest canopies on the climate at the snow surface. Simple algorithms are developed and used to adjust climate data collected above forest canopies to the snow surface. A 2-layer coupled energy- and mass-balance snowmelt model is used to simulate the deposition and ablation of the snowpack at five forested sites within the Canadian boreal forest for the 1994-1995 snow season. Results of the snowcover simulations indicate that the net snowcover energy balance remains close to zero for the winter months, but exhibits a sharp increase in the spring months. The rapid energy gain in the spring is strongly controlled by canopy cover, and is dominated by net radiation fluxes, with minor contributions from sensible, latent, soil, and advected energy fluxes. Net snowcover irradiance dominates during the spring months due to increased solar intensity and longer day lengths, coupled with increased radiation transmission through canopies at high sun angles, and reduced

snowcover albedo resulting from the deposition of fine organic debris. Turbulent (sensible and latent) energy fluxes comprise a relatively minor portion of the net snowcover energy exchange, indicating that the sub-canopy snowcover is relatively insensitive to the meteorological parameters controlling these fluxes. The low thermal conductivity of organic-rich boreal soils must be considered for studies focusing on snowcover development when soil heat flux comprises a large portion of the snowcover energy balance. Model outputs at all sites generally show good agreement with measured snow depths, indicating that the techniques used in these investigations accurately simulate both the deposition and ablation of seasonal snowcovers. Results indicate that snowcovers in the boreal environment may be more sensitive to land-use transitions, rather than climate shifts, due to the strong control exerted by vegetation canopies on radiation transfer processes. The results also suggest that simple canopy adjustment algorithms may be effectively applied to spatially distributed snowcover simulations. More data is required to evaluate the accuracy of these methods for computing energy transfer within canopies having significantly different structures than the sites used in this study.

Seasonal Snowcover Dynamics Beneath Boreal Forest Canopies

by

Timothy E. Link

A THESIS

submitted to

Oregon State University

in partial fulfillment of
the requirements for the
degree of

Master of Science

Presented June 29, 1998
Commencement June 1999

Master of Science thesis of **Timothy E. Link** presented on **June 29, 1998**

Approved:

Redacted for Privacy

Co-Major Professor, representing Geology

Redacted for Privacy

Co-Major Professor, representing Geology

Redacted for Privacy

Chair of Department of Geosciences

Redacted for Privacy

Dean of Graduate School

I understand that my thesis will become part of the permanent collection of Oregon State University libraries. My signature below authorizes release of my thesis to any reader upon request.

Redacted for Privacy

Timothy E. Link, Author

ACKNOWLEDGMENTS

I would like to thank Danny Marks for his constant support and encouragement throughout the duration of this research. I would also like to thank Julia Jones, Gordon Grant, Mike Unsworth, Peter Clark, and Herb Huddleston for their comments and suggestions in the preparation of this document. I am indebted to James Domingo and Debi Stritzke, who managed to fix even the most bizarre computer problems over the past few years. Meteorological data were provided by the diligent work of many people within the Saskatchewan Research Council. Special thanks go to the observers for their assistance with this project. Sub-canopy radiation, wind, and temperature measurements were collected by Janet P. Hardy and Robert E. Davis, of the Cold Regions Research and Engineering Laboratory (CRREL). The snow course data in the SSA were collected by the study area manager Mary Dalman, assisted by Vivian Heap. The NSA snow courses were carried out by AES Weather Specialist Bill Palmer, assisted by Martha Evaluardjuk. Site location maps are provided courtesy of the BOREAS Information System (http://boreas.gsfc.nasa.gov). Funding for this research was provided by NASA, (grant no. NAG5-2301); reference no. 2207-BOREAS-U107). Office and computing facilities were provided by the U.S. Environmental Protection Agency, Western Ecology Division. I would finally like to express my extreme gratitude to Sharyl, Quixo, and Sam Kammerzell for their constant support and tolerance of overly technical terms used to describe simple phenomena.

Table of Contents

List of Figures

List of Tables

List of Notation

C_{p_p} specific heat of precipitation (J kg^{-1} K^{-1}).
C_p specific heat of air (1005 J kg^{-1} K^{-1}).
E mass flux by evaporation or condensation from the snow surface (kg m^{-2} s^{-1}).
G heat transfer by conduction and diffusion between snow cover and soil (W m^{-2}).
H sensible heat exchange (W m^{-2}).
K_H bulk transfer coefficient for heat (J m^{-1} K^{-1} s^{-1}).
K_W bulk transfer coefficient for water vapor (J m^{-1} K^{-1} s^{-1}).
K_{es} effective thermal conductivity of snowcover (J m^{-1} K^{-1} s^{-1}).
K_{eg} effective thermal conductivity of soil (J m^{-1} K^{-1} s^{-1}).
L incoming thermal radiation (W m^{-2}).
L_c thermal radiation by a forest canopy (W m^{-2}).
L_o above-canopy thermal radiation (W m^{-2}).
L_f sub-canopy thermal radiation (W m^{-2}).
L_n net thermal radiation (W m^{-2}).
L_v latent heat of vaporization of water (2.5×10^6 J kg^{-1}).
L_vE latent heat exchange (W m^{-2}).
M heat transfer by advection (W m^{-2}).
ΔQ change in snow cover energy (W m^{-2}).
R_n net all-wave radiation (W m^{-2}).
S_b direct solar radiation (W m^{-2}).
$S_{b,f}$ sub-canopy direct solar radiation (W m^{-2}).
$S_{b,o}$ above-canopy direct solar radiation (W m^{-2}).
S_d diffuse solar radiation (W m^{-2}).
$S_{d,f}$ sub-canopy diffuse solar radiation (W m^{-2}).
$S_{d,o}$ above-canopy diffuse solar radiation (W m^{-2}).
S_g global solar radiation (W m^{-2}).
$S_{g,f}$ sub-canopy global solar radiation (W m^{-2}).
$S_{g,o}$ above-canopy global solar radiation (W m^{-2}).
S_n snowcover net solar radiation (W m^{-2}).
$S_{n,f}$ sub-canopy snowcover net solar radiation (W m^{-2}).
T_a air temperature (K or °C).
$T_{a,f}$ sub-canopy air temperature (K or °C).
T_c canopy temperature (K or °C).
T_g soil temperature (K or °C).
T_{pp} precipitation temperature (K or °C).
T_s snow surface temperature (K or °C).

e_a vapor pressure of the air (Pa).
h_c vegetation canopy height (m).

List of Notation (continued)

q	specific humidity in air (Pa).
q_s	specific humidity at the snow surface (Pa).
rh	relative humidity (dimensionless).
t_{step}	length of timestep (s)
u_f	sub-canopy wind speed (m s^{-1}).
u_o	super-canopy wind speed (m s^{-1}).
z_g	depth below soil surface of soil temperature measurement (m).
z_{pp}	depth of precipitation (m).
z_s	depth of snowcover (m).
α_b	direct albedo (dimensionless).
α_d	diffuse albedo (dimensionless).
α_{nir}	near-infrared (0.28-0.7 μm) albedo (dimensionless).
α_{vis}	visible (0.7-2.8 μm) albedo (dimensionless).
ε_c	canopy surface emissivity (variable, dimensionless).
ε_s	snow surface emissivity (~0.99, dimensionless).
μ	canopy optical extinction coefficient (m^{-1}).
θ	Solar zenith angle (90- β, degrees).
ρ_a	density of air (kgm^{-3}).
ρ_{pp}	density of precipitation (kg m^{-3}).
σ	Stefan-Boltzman constant (5.6697×10^{-8} W m^{-2} K^{-1}).
σ_b	canopy forward scattering coefficient for direct irradiance (dimensionless).
τ_d	canopy optical transmissivity for diffuse radiation (dimensionless).
τ_L	canopy optical transmissivity for thermal radiation (dimensionless).

AGCM	Atmospheric General Circulation Model
AMS	Automated Meteorological Station
BOREAS	Boreal Ecosystem Atmosphere Study
FAVD	Foliage Area Volume Density
GORT	Geometric-Optical Radiative Transfer
IFC	Intensive Field Campaign
LSP	Land Surface Parameterization
NIR	Near Infrared
NSA	Northern Study Area
OA	Old Aspen
OBS	Old Black Spruce
OJP	Old Jack Pine
SRC	Saskatchewan Research Council
SSA	Southern Study Area
SWE	Snow Water Equivalent
YTH	mixed Spruce/Poplar

Seasonal Snowcover Dynamics Beneath Boreal Forest Canopies

Introduction

The boreal forest is the largest terrestrial biome, covering approximately 15% of the surface of the Earth (Pomeroy and Dion, 1996). Recent studies indicate that climate changes occurring as a result of increased atmospheric CO_2 will be most pronounced at higher latitudes (45° - 65° N), leading to warming and drying of the boreal regions (Schlesinger and Mitchell, 1987, Bonan et al., 1992). There is evidence that these regions currently function as a sink for carbon released by fossil fuel combustion and land-use changes (Tans et al., 1990), but climate change may substantially alter carbon dynamics in the boreal regions (Sellers et al., 1995). The seasonal onset of carbon assimilation and soil respiration in the boreal forest is strongly controlled by the timing of snowpack ablation and subsequent soil warming (Sellers et al., 1995). An understanding of the geophysical processes controlling snowcover deposition and ablation is therefore critical to the quantification of water and carbon dynamics within the boreal ecosystem.

The Boreal Ecosystem-Atmosphere Study (BOREAS) was undertaken in 1993, as a multi-disciplinary, international field investigation to improve the scientific understanding of the mass and energy transfer processes between boreal forests and the lower atmosphere (BOREAS Explan, 1995). An associated objective of the project is to improve process models describing these dynamics, and to develop techniques for applying the models over large spatial scales. These developments will ultimately lead to improved land surface parameterizations (LSPs), which will be used to drive atmospheric general circulation models (AGCMs), in order to improve global climate change analyses (Sellers et al., 1997).

Seasonal snowcover dynamics respond to climate conditions at the snow surface, which are locally controlled by topographic and vegetation variations. Topographic relief is relatively subtle in many boreal regions, therefore climate conditions at the snow

surface are primarily controlled by variations in the overlying vegetation canopy. The accurate adjustment of climate data collected at open sites for the presence of various vegetation canopies is therefore critical for the numerical modeling of snowcover processes in the boreal environment, to understand the seasonal dynamics of mass- and energy-transfer in this system.

This study approaches the problem of simulating snowcover processes beneath forest canopies by developing a series of simple canopy adjustment algorithms which can be applied to time-series meteorological data collected above forest canopies, or at open sites. The algorithms are designed to require a minimum of commonly available spatial data products, so that the techniques may be readily applied in areas where detailed canopy measurements are not available. The algorithms are tested in conjunction with a 2-layer mass- and energy-balance snowmelt model (SNOBAL) to simulate the development and ablation of seasonal snowcovers beneath a range of forest canopies. The resulting techniques represent one approach which may ultimately be used to simulate snowcover processes within heterogeneous forested regions. This approach may therefore help to assess the potential effects of altered land-use patterns and climate conditions on hydrologic processes and ecosystem dynamics.

Objectives

The primary goal of this investigation is to accurately simulate the energy- and mass -balance of the seasonal snowcover over an entire snow season at several locations beneath a range of boreal forest canopies. The specific objectives of this investigation are to:

1.) Use above- and below-canopy climate data from the BOREAS study to analyze how forest canopies modify climate conditions at the snow surface, relative to above-canopy climate conditions.

2.) Develop a series of simple algorithms based on the analyses of canopy effects to adjust climate conditions measured above forest canopies, or in open areas to conditions at the forest floor.

3.) Use canopy-corrected meteorological data to drive a 2-layer mass- and energy-balance snowmelt model (SNOBAL) developed by Marks, (1988), to simulate the development and ablation of the seasonal snowpack beneath boreal forest canopies.

4.) Validate the model results using both automatically and manually collected snow depth measurements.

5.) Develop an understanding of the sub-canopy snowcover dynamics within the boreal forest, based on modeled and measured snowpack properties.

6.) Determine the data required to spatially distribute the canopy adjustment algorithms, and identify potential problems associated with using simple canopy adjustment over heterogeneous areas.

Background

Canopy Effects

The presence of a forest canopy overlying a seasonal snowcover alters the processes of mass and energy transfer and snowpack properties relative to open sites (Figure 1). During snowpack deposition, the canopy intercepts a portion of the incoming snow (Schmidt and Gluns, 1991; Sturm, 1992; Troendle and King, 1985), which later may fall to the ground, increasing the snowpack density, or it may sublimate, melt or evaporate from the canopy depending on climate conditions (Golding and Swanson, 1986; Lundberg and Halldin, 1994).

Forest canopies strongly influence the snowcover energy balance, by absorbing and reflecting incoming solar radiation (0.3 - 2.8 μm), and by altering the emission of thermal radiation (2.8 - 100 μm) (Male and Granger, 1981; Lafleur and Adams, 1986). The relative importance of shading and emissivity alteration is a function of the canopy height and density, and of the optical transmissivity of the individual trees. The forest canopy is also a source of fine organic debris which contaminates the snowcover, thereby decreasing the albedo relative to less contaminated open areas (Pomeroy and Dion, 1996). Previous studies (Marks and Dozier, 1992; Male and Granger, 1981), noted that net radiation is the most important component controlling snowpack ablation, therefore the accurate quantification of canopy effects on radiative transfer processes are critical to modeling snowcover processes beneath forest canopies.

Forest canopies reduce wind velocities relative to above-canopy and open sites (Jones, 1992). Air temperature and vapor pressure beneath a forest canopy can also vary relative to open, or above-canopy locations. A forest cover shelters the snowcover from wind, and alters the temperature and humidity gradients, greatly reducing the efficiency of turbulent energy transfer (Berris and Harr, 1987; Ohta et al., 1993, Marks et al., in

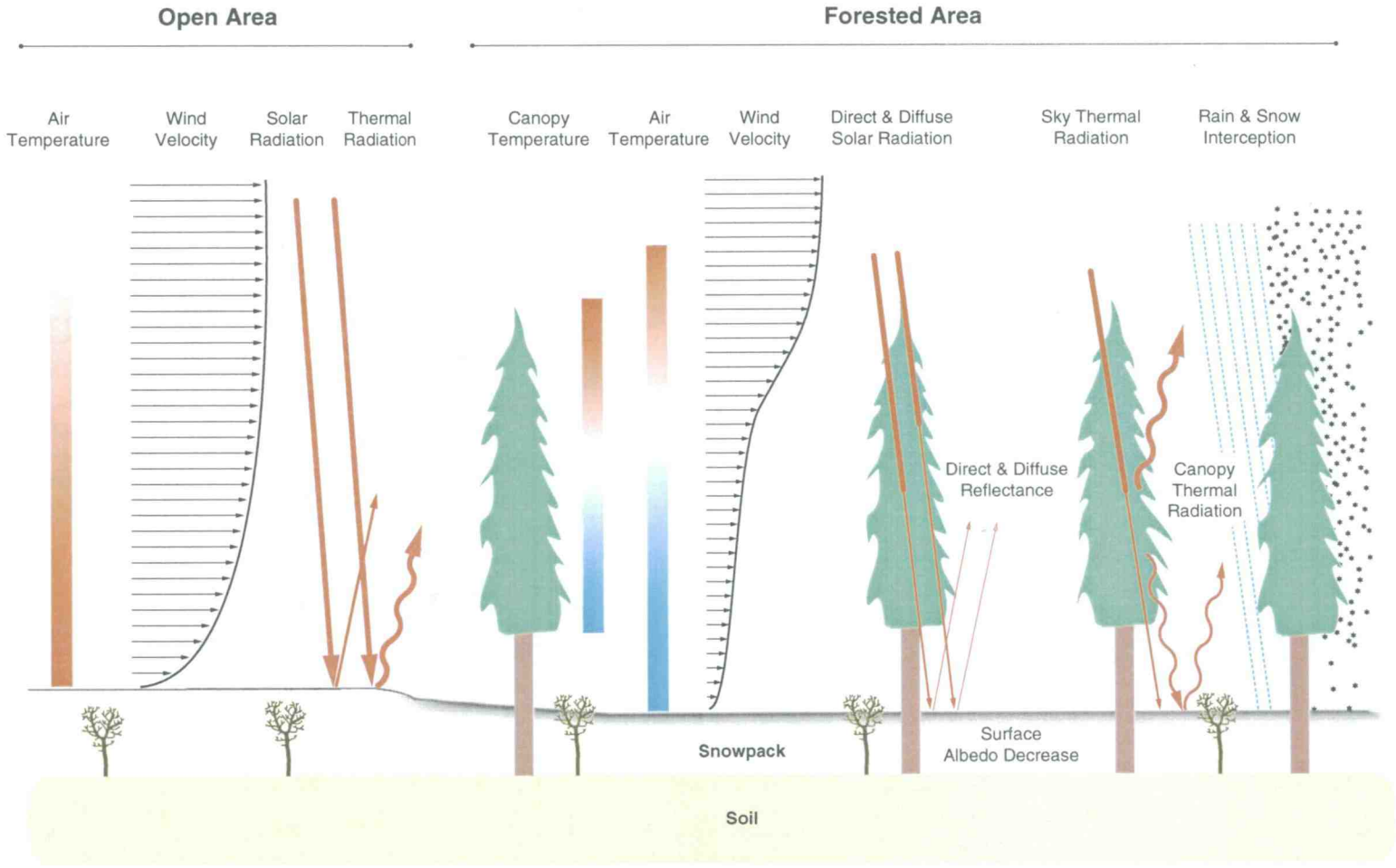

Figure 1. Conceptual diagram of forest canopy effects on the microclimate at the snow surface.

press). It is important to consider such alterations of micrometeorological conditions beneath forest canopies when simulating snowcover dynamics in forested systems.

Prior Work

A 50-day snowcover ablation period was successfully simulated beneath a variety of boreal forest canopies using the multi-layer mass and energy balance snowmelt model SNTHERM (Jordan, 1991) driven with data collected during the BOREAS experiment (Hardy et al., 1997). The solar radiation above the canopies was adjusted to the snow surface using a hybrid geometric-optical and radiative transfer (GORT) model (Ni et al., 1997). The GORT model treats the forest canopy as an assemblage of randomly distributed ellipsoidal crowns, and is parameterized by a horizontal to vertical crown ratio, foliage area volume density (FAVD), stem density, and crown depth. The model explicitly treats the transmission of beam radiation through canopy gaps, diffuse radiation through gaps, and radiation scattered by the canopy elements to provide accurate estimates of radiation within discontinuous canopies. The GORT model also accounts for the optical anisotropy of tree crowns arising from the horizontal branch whorls, to accurately simulate radiation transfer at all solar elevation angles.

In the simulations completed by Hardy et al. (1997), between- and within-crown openness factors determined by GORT were summed to estimate the proportion of hemispherical area composed of sky and canopy above the snow surface. Thermal radiation at the snow surface was then determined from measured open values, and canopy emission values calculated from measured within canopy air temperature, each adjusted by the appropriate proportion of canopy and sky.

Results from the SNTHERM simulations agreed with observations that complete ablation occurs first in open areas, followed by areas beneath individual trees, and finally by small gaps between trees. During the ablation period, net radiation was found to be the primary energy balance component, with counteracting sensible and latent energy fluxes similar in magnitude, but opposite in direction. A parametric study of snowcover ablation beneath boreal conifer forest canopies of varying densities revealed that net radiation dominates the energy balance at all canopy densities (Davis et al., 1997).

However, the timing of the radiation shift from negative to positive fluxes was strongly dependent on the canopy characteristics. Consequently, modeled melt rates varied by a factor of five between the minimum and maximum density classes, when using the median tree height. A delay of approximately 10 days in the onset of seasonal snowmelt between the northern and southern BOREAS study areas was both observed and simulated using SNTHERM.

SNOBAL was successfully used to simulate the ablation of seasonal snowcovers in a variety of alpine environments (Marks, 1988; Susong et al., 1996; Garen and Marks, 1996). SNOBAL also successfully simulated both the development and ablation of snowcovers in both open and forested areas under a wide range of climate conditions (Marks et al., in press, Risley et al., 1997). The simulation of snowcover development is advantageous because no knowledge of snowpack properties are required to initialize the model run; snowcover properties are computed by the model from standard meteorological data.

Several key differences exist between the modeling approach presented herein, and previous modeling investigations in the boreal forest. These investigations focus on the dynamics of snowcovers over an entire season, rather than on solely the ablation period. Snowcover processes are investigated beneath a variety of canopy structures, ranging from deciduous, through mixed deciduous/conifer, to dense conifer. Meteorological adjustments for the forest canopies are very simple, spatially distributable techniques, which are parameterized with commonly available or easily derivable spatial data, rather than specialized empirical measurements. SNOBAL is a relatively simple 2-layer snowcover model, which can be driven using commonly available climate data. Although these techniques may not be as accurate as the more complex radiative transfer and snowcover models used in other studies, the ability to easily simulate an entire season beneath a variety of land cover types, represents a valuable step towards assessing the hydrologic effects of land use and climate change on forested systems.

Approach

Seasonal mass and energy-balance snowcover simulations beneath boreal forest canopies with a range of structures were completed using the following procedure:

1.) Identify point locations at which to complete simulations.

2.) Identify and evaluate the data to be used for the development of canopy adjustments algorithms, model forcing and validation.

3.) Use basic environmental physics theory to develop a series of simple canopy correction algorithms that can be applied to canopies of differing structures.

4.) Adjust the continuous time-series meteorological data records using both the canopy algorithms, and existing numerical models.

5.) Simulate the mass- and energy-balance dynamics of the seasonal snowcover at each site using the numerical model SNOBAL developed by Marks (1988) and later improved and refined by Marks and Dozier (1992), Garen and Marks (1996), Susong et al., (1996), and Marks et al., (in press).

Site Descriptions

The BOREAS study region is an area 1000 km × 1000 km in size, which comprises most of Saskatchewan and Manitoba (Figure 2). This region contains a northern and southern study area (NSA and SSA) which are 100 km × 80 km and 130 km × 90 km, respectively. The NSA is close to the northern limit of the closed crown boreal forest, and is typical of extreme northern boreal forests. The forest is predominantly composed of Black Spruce, with some stands of Jack Pine, and some stands of mixed deciduous and conifer species. The SSA is located approximately 780 km south-west of the NSA, near the southern extent of the boreal forest. The SSA is mainly composed of Aspen groves, Black Spruce and Jack Pine stands, open meadows and grasslands.

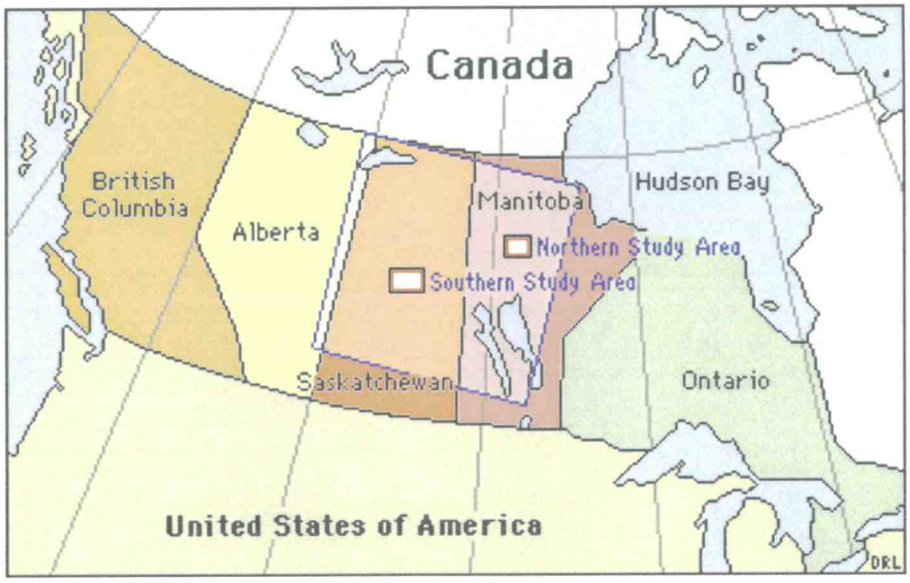

Figure 2. Location of the BOREAS study region.

Two sites in the NSA, and three sites in the SSA were selected for snowcover mass and energy balance simulations. The locations were chosen to cover the range of canopy characteristics (i.e deciduous through dense conifer) found in the boreal regions, and upon the completeness and availability of meteorological data for both model forcing and validation. In the NSA, sites beneath a mature Jack Pine (NSA-OJP) and a mixed Spruce / Poplar (NSA-YTH) canopy were selected. In the SSA, sites located beneath mature Aspen (SSA-OA), mature Jack Pine (SSA-OJP) and mature Black Spruce (SSA-OBS) forest canopies were selected. Each site is flat, with a laterally continuous (up to ~1km) and homogeneous canopy with respect to species composition, stand age, and stem density. Site locations and elevations are listed in Table 1. Site locations within the NSA and SSA are shown in Figures 3 and 4.

Data Collection

Climate data records within the BOREAS study region consist of continuous measurements collected both above and below a range of forest canopy covers. In addition, climate and snowcover conditions beneath several canopy types were monitored during several week long intensive field campaigns (IFCs). These unique, vertically

Table 1. Site Locations

Site	Latitude	Longitude	Elevation (m)
SSA			
OJP	53.916° N	104.69° W	511
OA	53.629° N	106.20° W	587
OBS	53.985° N	105.12° W	629
NSA			
OJP	55.927° N	98.62° W	282
YTH	55.750° N	97.87° W	221

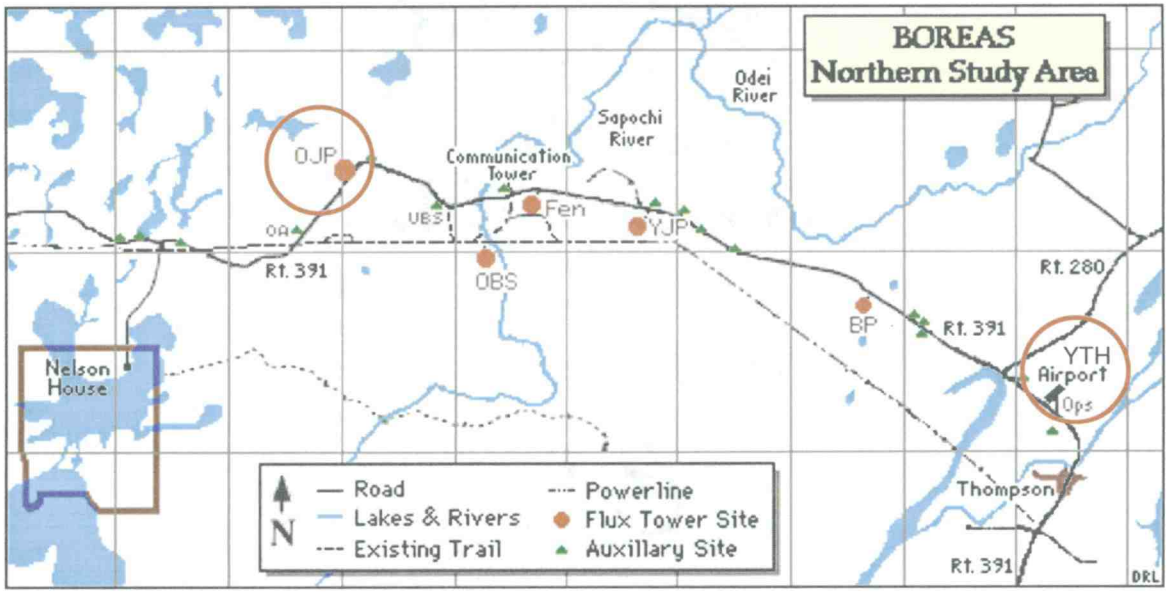

Figure 3. Location of Northern Study Area (NSA) sites.

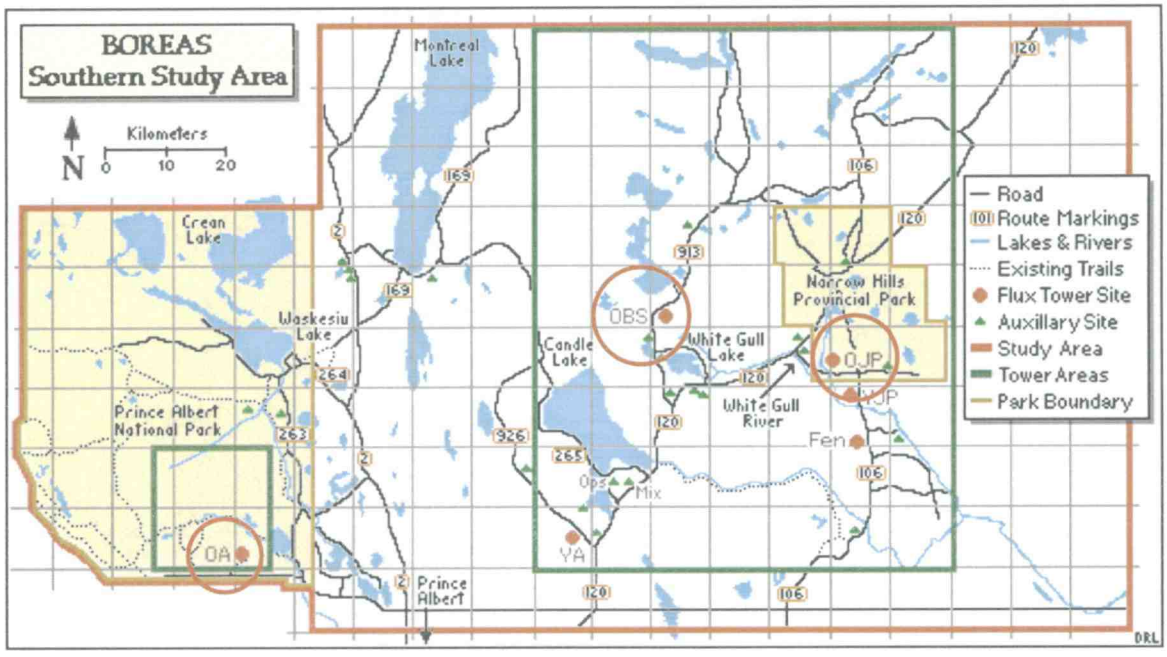

Figure 4. Location of Southern Study Area (SSA) sites.

distributed and temporally extensive data records permit both the derivation and validation of canopy adjustment algorithms, and provide the necessary forcing and validation data for mass- and energy-balance snowcover simulations in the boreal environment.

Continuous meteorological data for the NSA-YTH, NSA-OJP, SSA-OJP, and SSA-OA sites were obtained from automated meteorological stations (AMS) maintained by the Saskatchewan Research Council (SRC) to support BOREAS investigations (Shewchuk, 1997). At each site, the suite of parameters listed in Table 2 were recorded as 15 minute averages of sensor scans completed every 5 seconds. Above-canopy sensor suites are located from 3 to 6 m above the top of the canopy, and below-canopy instrumentation is located at 2 m above ground level. Although no continuously monitored sensors were installed at the SSA-OBS stand, this location was included in the analyses, due to the large proportion of area represented by this canopy type, and availability of sub-canopy radiation data. Meteorological data for SSA-OBS was substituted from the nearest AMS, located at the SSA-OJP site, approximately 30 km to the east, for all calculations and model runs.

Table 2. BOREAS Instrumentation Summary

Parameter	Sensor Location	Sites	Period of Record Resolution	Manufacturer Model
Forcing Data				
Net Solar Radiation	above-canopy	NSA: OJP, YTH SSA: OJP, OA	continuous 15 minute	Eppley PSP Precision Spectral Pyranometer
Diffuse Solar Radiation	above-canopy	NSA: OJP SSA: OJP, OA	continuous 15 minute	Eppley PSP Precision Spectral Pyranometer with Eppley Shadow Band Stand
Incoming Thermal Radiation	above-canopy	NSA: OJP SSA: OJP, OA	continuous 15 minute	Eppley PIR Precision Infrared Radiometer
Canopy Temperature	above-canopy	NSA: OJP, YTH SSA: OJP. OA	continuous 15 minute	Everest Interscience 4000AL Infrared Thermometer
Wind Velocity	above-canopy	NSA: OJP, YTH SSA: OJP, OA	continuous 15 minute	R.M. Young 05103-10 Wind Monitor
Relative Humidity	above-canopy	NSA: OJP, YTH SSA: OJP, OA	continuous 15 minute	Campbell Scientific HMP35CF Temperature/Relative Humidity Probe
Air Temperature	within-canopy	NSA: OJP, YTH SSA: OJP, OA	continuous 15 minute	Campbell Scientific 107F Temperature Probe
Soil Temperature	0.5 m depth	NSA: OJP, YTH SSA: OJP, OA	continuous 15 minute	Campbell Scientific 107BAM Temperature Probe
Precipitation	small clearing	NSA: OJP, YTH SSA: OJP, OA	continuous 15 minute	Belfort Instrument Company Rainfall Transmitter

Table 2. BOREAS Instrumentation Summary (continued)

Parameter	Sensor Location	Sites	Period of Record Resolution	Manufacturer Model
Validation Data				
Snow Depth	small clearing	NSA: OJP, YTH SSA: OJP, OA	continuous 15 minute	Campbell Scientific UDG01 Ultrasonic Depth Gauge
Snow Depth	open and below-canopy	*SSA: Aspen, Black Spruce, Jack Pine	bi-monthly	ESC-30 snow sampler
Net Solar Radiation	below-canopy	SSA: OJP	2/7 - 2/11, 1994 10 minute	10 Eppley PSPs
		SSA: OBS	2/28 - 3/4, 1996 1 minute	
		SSA: OA	3/4 - 3/8, 1996 1 minute	
Incoming Thermal Radiation	below-canopy	SSA: OBS	2/28 - 3/4, 1996 1 minute	2 Eppley PIRs
		SSA: OA	3/4 - 3/8, 1996 1 minute	
Wind Velocity	below-canopy	SSA: OJP	2/7 - 2/11, 1994 10 minute	R.M. Young 05103-10 Wind Monitor

***NOTE:** Manual snow depth measurements were located in areas deemed to be representative of typical land covers, and were not co-located at sites where continuous meteorological parameters were recorded.

Sub-canopy solar radiation measurements were made during winter IFCs completed in 1994 and 1996, according to procedures described in detail by Hardy et al., (1997). An array of 10 Eppley pyranometers were randomly located beneath the forest canopies, so that some radiometers were adjacent to stems, and others were located in canopy gaps, to achieve a spatially integrated measure of global solar radiation at the snow surface. Measurements were made over periods of three to four clear days, with radiometers randomly relocated once a day. Ten minute averages of 1 minute readings were recorded at SSA-OJP, and 1 minute readings were recorded at SSA-OA and SSA-OBS. Measurements at SSA-OJP, SSA-OA, and SSA-OBS were completed over February 7-11, 1994, March 4-8, 1996, and February 28-March 3, 1996, respectively. During these time periods, the maximum solar elevation angle at the sites was approximately 22° for SSA-OJP, and 29° for SSA-OA, and SSA-OBS.

Measurements of sub-canopy thermal radiation were completed using two Eppley pyrgeometers, during the 1996 IFCs at the SSA-OA and SSA-OBS sites. In addition, at SSA-OA, two measurements of tree trunk temperatures near the snow surface, and one measurement of the snow surface temperature was recorded using an infrared thermometer. At SSA-OBS, 2 measurements of canopy temperature, and 1 measurement of trunk temperature was completed using the infrared sensors. At the SSA-OJP site, sub-canopy wind speed measurements were completed with an R.M. Young wind monitor located 2 m above the snow surface concurrently with the collection of solar radiation data. Manual snow course depth, density, and SWE measurements were also completed within 4 land cover types (open, Aspen, Black Spruce, and Jack Pine) in the SSA, and 1 land cover type (Jack Pine/Poplar) in the NSA. Each snow course consisted of 5 stations approximately 100 m apart, where snow measurements were repeated near the 1st and 15th of the winter and spring months. All density measurements were completed with a large diameter ESC-30 snow sampler with a 30 cm^2 cutter area, and a spring balance. The snow depths at each site were recorded to the nearest 0.5 cm, and the 5 sites averaged to obtain a mean snow depth for each land cover type.

Development of Canopy Adjustment Algorithms

SNOBAL numerically describes the physics of energy transfer at the snow surface, given meteorological measurements taken at, or near the snow surface. The presence of a vegetation canopy over a snow surface alters the climate conditions at the snow surface relative to open, or above-canopy locations as described above (Figure 1). The presence of a forest canopy necessitates the modification of the raw meteorological data streams required to drive SNOBAL. The above-canopy solar radiation data must be adjusted to account for shading of the snow surface by the vegetation canopy, and for snowcover albedo, to obtain the net solar radiation absorbed by the snowpack. The above-canopy thermal radiation data must also be adjusted to account for the modification of incoming thermal radiation by the forest canopy. Windspeeds measured above the forest canopy must be modified to account for the sheltered conditions present at the forest floor, in order to accurately calculate the turbulent energy fluxes. Basic environmental physics theory is combined with measurements taken above and below the various canopy covers to analyze how forest canopies alter climate conditions at the snow surface, and provide information for the development of simple algorithms to adjust climate data for the presence of variable canopy covers.

Net Solar Radiation

The transmission of solar radiation through a vegetation canopy is dependent on the relative proportions of the beam and diffuse components, spectral characteristics of incoming radiation, and the physical structure and reflectance of the vegetation (Monteith and Unsworth, 1990). The adjustment algorithms for solar radiation use basic canopy characteristics to calculate the contribution of the different radiation components. Transmission through individual canopy elements (e.g. gaps, crowns, stems), and spectral properties of transmitted solar radiation are not explicitly considered, in order to limit both the driving and validation data required for the algorithms.

Theory

Global solar radiation (S_g) is composed of a diffuse (S_d), or non-directional component, and a collimated, or beam (S_b) component, expressed as:

$$S_g = S_d + S_b \quad [1]$$

The diffuse radiation at the snow surface is expressed:

$$S_{d,f} = \tau_d \times S_{d,o} \quad [2]$$

where:

$S_{d,f}$ is the diffuse radiation at the snow surface (W m^{-2}),
$S_{d,o}$ is the diffuse radiation at the top of the canopy (W m^{-2}), and
τ_d is the optical transmissivity of the canopy to diffuse radiation (dimensionless).

This equation assumes that all diffuse radiation at the snow surface originates as diffuse radiation at the top of the canopy. However, a proportion of the diffuse radiation at the snow surface may result from forward scattering of beam radiation by the canopy elements. The above equation can be expanded:

$$S_{d,f} = (\tau_d \times S_{d,o}) + (\sigma_b \times S_{b,o}) \quad [3]$$

where:

$S_{b,o}$ is the beam radiation at the top of the canopy (W m^{-2}), and
σ_b is the proportion of beam radiation scattered toward the snow surface by the canopy (dimensionless).

For the purposes of describing radiation transmission for modeling snowcover processes, we usually assume that the canopy elements scatter a negligible proportion of the beam radiation due to the highly absorptive nature of the canopy elements. However, accurate derivation of optical canopy constants for relatively reflective canopy types such as Aspen, requires the consideration of forward radiation scattering.

If it is assumed that the forest canopies present at the study locations are homogeneous and continuous, the transmission of beam radiation can be approximated using the Beer-Bouger-Lambert Law, which describes the exponential decay of radiation

through an isotropic, homogeneous medium (Peixoto and Oort, 1992). By applying this law, the beam radiation at a sub-canopy location ($S_{b,f}$) can be written as:

$$S_{b,f} = S_{b,o} e^{-\mu l} \qquad [4]$$

where:

l is the path length of the incoming solar beam through the canopy (m), and
μ is the extinction coefficient (m^{-1}), which is inversely proportional to the optical transmissivity of the canopy to beam radiation.

Since we assume that the canopy is uniform and infinite in all directions, l can be described by the trigonometric relationship:

$$l = h \sec(\theta) \qquad [5]$$

where:

h is the canopy height (m), and
θ is the solar zenith angle (°)

The beam solar radiation at the snow surface can be described by combining Equations [4] and [5]:

$$S_{b,f} = S_{b,o} e^{-\mu h \sec(\theta)} . \qquad [6]$$

Multiple scattering is not explicitly considered in these formulations, but is inherently accounted for in the empirical derivations of τ and μ. Studies of radiation transfer in snow-covered boreal forests indicate that intercepted snow has a negligible effect on radiation extinction within boreal conifer canopies (Pomeroy and Dion, 1996). We therefore assume that no adjustment to the radiation transfer algorithms are necessary to account for intercepted snow load.

In the above equations, $S_{g,o}$ and $S_{d,o}$ can be measured directly, and $S_{b,o}$ can be obtained by computing the difference. The global solar radiation below the canopy ($S_{g,f}$) is much more difficult to measure continuously at a site, due to the high spatial variability of radiation beneath forest canopies, and the high cost and effort associated

with maintaining a large array of radiometers. $S_{g,f}$ can be calculated by summing Equations [3] and [6], given sufficient information regarding the physical characteristics of the canopy. The height of the canopy is easily measured, and θ can be calculated based on solar geometry, leaving τ_d and μ to either be estimated, or determined empirically. At the SSA-OJP, SSA-OA, and SSA-OBS sites, the availability of high quality, high temporal resolution above- and below-canopy radiation measurements permits the accurate estimation of these two parameters.

Calculation of τ_d and σ_b

For conifer canopies, it is assumed that negligible forward scattering of beam radiation occurs, so that Equation [1] can be used to describe the transmission of diffuse radiation. This assumption is reasonable given the low albedo and texturally rough physical characteristics of the conifer canopies. Although $S_{d,f}$ measurements were not completed at any of the sites, individual radiometers within the sub-canopy array are occasionally shaded by canopy elements over the course of a day, yielding sporadic measurements of sub-canopy diffuse radiation. When all radiation data from the sub-canopy array is plotted synchronously, an approximate diffuse radiation curve is produced by the inverted peaks on the individual curves. τ_d is determined graphically, by iteratively multiplying $S_{d,o}$ by estimated values for τ_d, until the resulting curve matches the approximate $S_{d,f}$ curve to within 5%.

In the Aspen canopy, the assumption of minimal forward scattering of beam radiation may be invalid, due to the relatively smooth and reflective nature of the canopy. In this case, Equation [3] more accurately describes the transmission of diffuse radiation. The first partial day of sub-canopy radiation measurements at the Aspen site was cloudy, therefore all solar radiation measurements are composed entirely of diffuse radiation. In this case, τ_d is determined by computing the ratio of $S_{d,o}$ to $S_{d,f}$, integrated over the first partial day of measurements. The proportion of $S_{d,f}$ resulting from forward scattering of beam radiation is determined by subtracting $\tau_d S_{d,o}$ from $S_{d,f}$ for each measurement. σ_b is

then determined using a technique similar to the one described above, where iterative values for σ_b are multiplied by $S_{b,o}$ until a graphical solution is obtained.

Calculation of μ

$S_{b,f}$ for each time interval is computed by subtracting $S_{d,f}$, calculated using Equation [1] from the mean $S_{g,f}$ measured by the sub-canopy radiometer array. The total shortwave beam energy incident at the snow surface beneath the canopy during the sub-canopy measurement period is calculated by numerically integrating the $S_{b,f}$ over the measurement period, using the Simpson method. An iterative solution for μ is obtained for each canopy type by estimating values for μ, numerically integrating the calculated $S_{b,f}$ using Equation [6], until the resulting net incident energy matches the measured value to within 1%.

Algorithm Validation

Calculated $S_{g,f}$ values using Equations [3] and [6] over the period of sub-canopy radiation measurements are shown in Figures 5a-c. The average of the ten sub-canopy radiometers is depicted by the green line, and the calculated $S_{g,f}$ values are shown in red. The average radiometer traces exhibit some noise, indicating that the number of radiometers in the sub-canopy array is insufficient to completely average the sub-canopy spatial variability. Because the adjustment algorithm for solar radiation is calibrated to the measured $S_{g,f}$ values, the magnitude of the calculated values closely match the measured values. The calculated values match closely at all sun angles, indicating that the canopy filters are robust across a variety of sun angles. The accurate quantification of radiation transmission as a function of zenith angle suggests that these algorithms will effectively account for seasonal variations in zenith angle, and will therefore be applicable throughout the entire snow season.

Albedo Adjustments

The net diffuse and beam radiation absorbed by the snowcover is a function of the respective spectrally-integrated albedoes for diffuse and beam radiation, and is written:

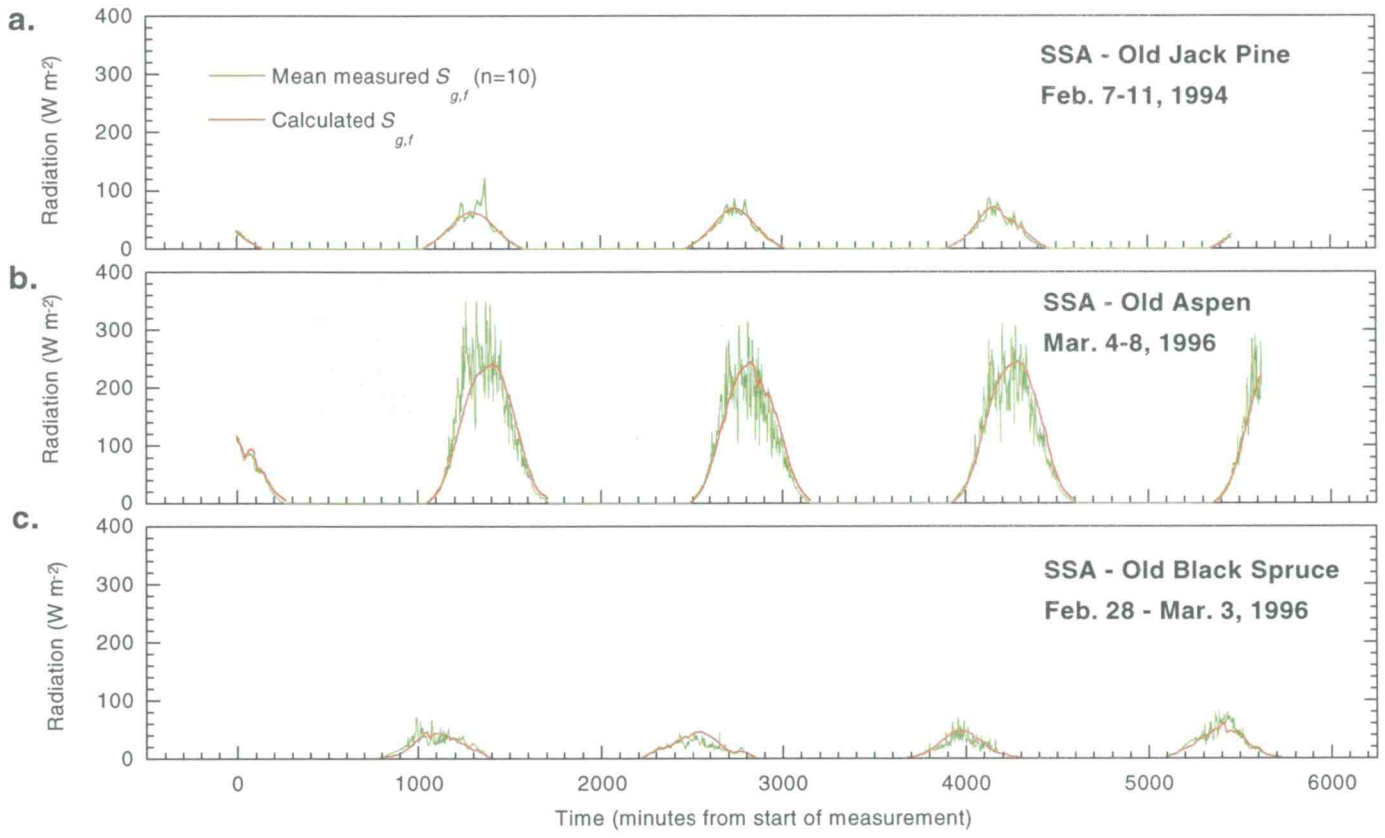

Figure 5. Measured and calculated sub-canopy solar radiation.

$$S_{n,f} = (1-\alpha_d)S_{d,f} + (1-\alpha_b)S_{b,f} \quad [7]$$

where:

α_d is the snowcover albedo for diffuse radiation (0.98, dimensionless),
α_b is the snowcover albedo for beam radiation (dependent on solar elevation angle),
$S_{d,f}$ is the diffuse radiation at the snow surface, and
$S_{b,f}$ is the beam radiation at the snow surface.

The snowcover albedo is a function of the spectral characteristics of the incoming radiation, snowpack grain size, moisture content and impurities (Warren and Wiscombe, 1980; Marks, 1988; Marks and Dozier, 1992). The albedo is also a function of solar zenith angle, such that the reflectance of solar radiation is greatest at high zenith angles. As a result, the diffuse albedo is typically slightly higher than the beam albedo due to the higher proportion of radiation reaching the surface from oblique angles (Male and Granger, 1981).

A constant open location α_d of 0.98 is applied to all calculated $S_{d,f}$ values to obtain the net diffuse radiation absorbed by the snowcover. The visible and near infrared beam albedoes (α_{vis} and α_{nir}, respectively) at each measurement interval for an open site are calculated as a function of grain growth and sunangle using the empirical relationships described by Warren & Wiscombe (1980), Wiscombe and Warren (1980), and Marshall and Warren (1987). The α_b was estimated from the average of α_{vis} and α_{nir}. At the forested sites, an additional albedo reduction function was applied to simulate the effects of organic debris accumulation within the snowpack. This function linearly decreases the albedoes from the time of maximum snowpack accumulation to the time of complete ablation. The function is optimized so that the sub-canopy snowcover albedo reaches a value of 0.55 just prior to complete ablation, consistent with observations from boreal forests (Pomeroy and Dion, 1996).

Thermal Radiation

Theory

The thermal radiation (0.7-2.8 μm) beneath forest canopies (L_f) is altered relative to the thermal flux at open sites (L_o) due to the blockage of sky thermal radiation, and emission of thermal radiation from the canopy elements. L_f is written:

$$L_f = \tau_L L_o + (1 - \tau_L) L_c \qquad [8]$$

where:

τ_L is the transmissivity of the canopy to thermal radiation (dimensionless),
L_o is the thermal radiation measured above the forest canopy (W m^{-2}), and
L_c is the thermal radiation emitted by the forest canopy (W m^{-2}).

If the canopy temperature is known, L_c can be calculated from the Stefan-Boltzman equation.

$$L_c = \varepsilon_c \sigma T_c^4 \qquad [9]$$

where:

ε_c is the emissivity of the canopy (0.96 dimensionless),
σ is the Stefan-Boltzman constant (5.6697×10^{-8} W m^{-2} K^{-1}), and
T_c is the mean surface temperature of the canopy (K).

Neglecting the negligible reflection of thermal radiation by the canopy, Equations [8] and [9] are combined to yield:

$$L_f = \tau_L L_o + (1 - \tau_L) \varepsilon_c \sigma T_c^4 \qquad [10]$$

Diffuse solar and thermal radiation are both non-directional, therefore, it is assumed that τ_d, calculated from the sub-canopy radiation measurements, is equal to τ_L. Forest canopies behave as almost perfect black bodies having emissivity values of approximately 0.96 (Price and Petzold, 1984). Using the scalar values for τ_L and ε_c, Equation [10] can be used to calculate L_f given values for L_o and T_c, assuming that the measured T_c values are representative of all canopy elements.

Algorithm Validation

Air and canopy element temperatures during the winter 1996 IFC at the SSA-OBS and SSA-OA sites are illustrated in Figures 6a and 7a. Corresponding measured above- and below-canopy radiation values and calculated canopy radiation values using Equation [10] are shown in Figures 6b and 7b.

Canopy and trunk temperature measurements at the SSA-OBS site are very similar throughout the measurement period, suggesting that the vegetation layer is relatively isothermal. Conifer canopies are structurally similar, therefore we assume that OJP canopies exhibit similar thermal characteristics for the purposes of snowmelt modeling. The thermal radiation was calculated at the OBS site using canopy temperatures substituted from the SSA-OJP site, due to the absence of an AMS within the Black Spruce canopy. Measured and calculated L_f values show close agreement during the entire sub-canopy measurement period, indicating that the L_f formulation provides reasonable estimates, when data from the OJP site are used. Differences between above- and below-canopy thermal radiation values vary by up to 25%, indicating the importance of accounting for the modification of the open site thermal radiation by forest canopies.

At the SA-OA site, the measured sub-canopy thermal radiation varies by approximately 30% relative to the above-canopy thermal radiation over the period of measurement. Initial calculated sub-canopy thermal radiation indicated good agreement with the measured sub-canopy thermal values for the daytime periods, but underpredicted radiation for the night periods by approximately 10%. Temperature measurements at this site indicate that trunk temperatures may exceed canopy temperatures by more than 10°C during night periods (Figure 7a). The observed departure between the calculated and measured values are most likely caused by the higher trunk temperatures, which may not be effectively viewed by the down-looking above-canopy IR thermometers. A simple correction for the emissivity enhancement by the Aspen trunks was implemented by increasing the measured canopy temperatures by 3°C. This adjustment provides a more accurate estimate of the diurnally integrated sub-canopy thermal radiation climate, by

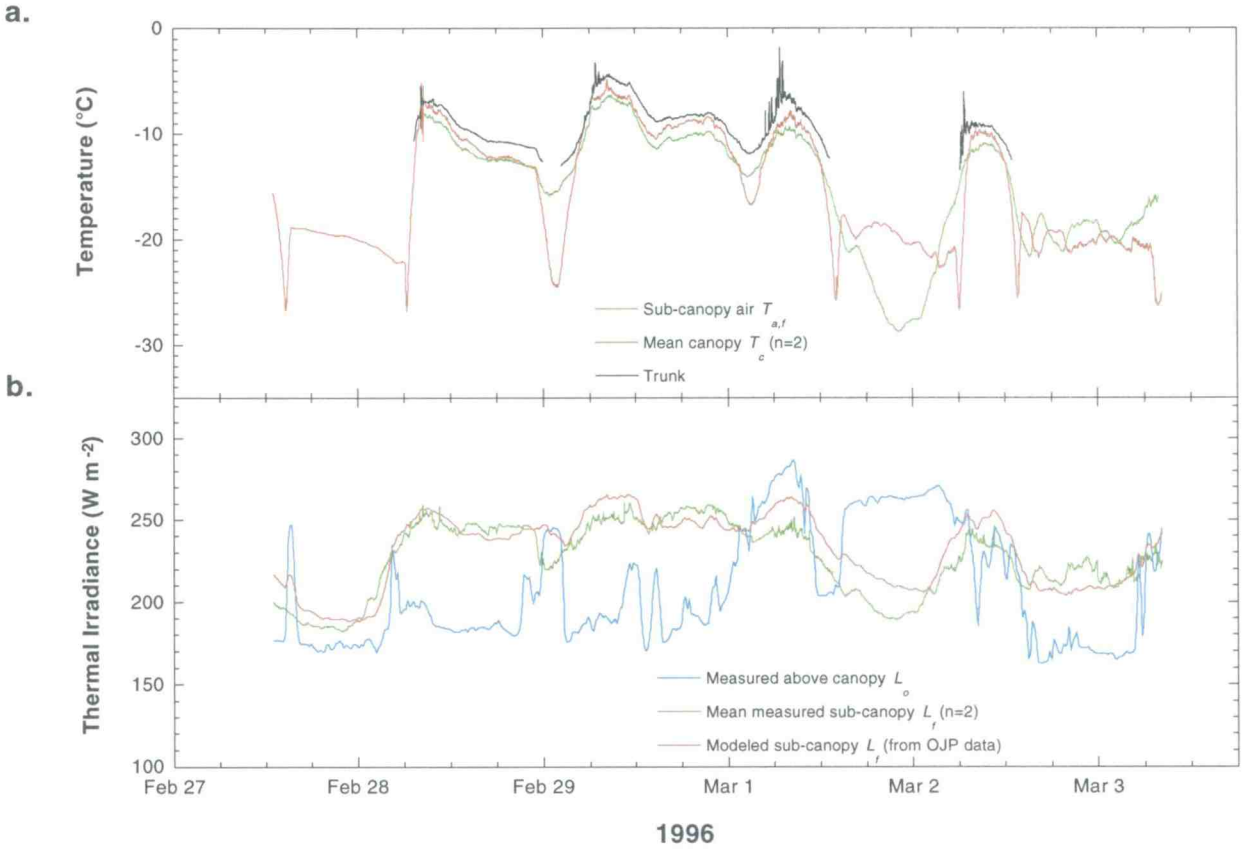

Figure 6. Temperatures and thermal radiation at the SSA OBS site.

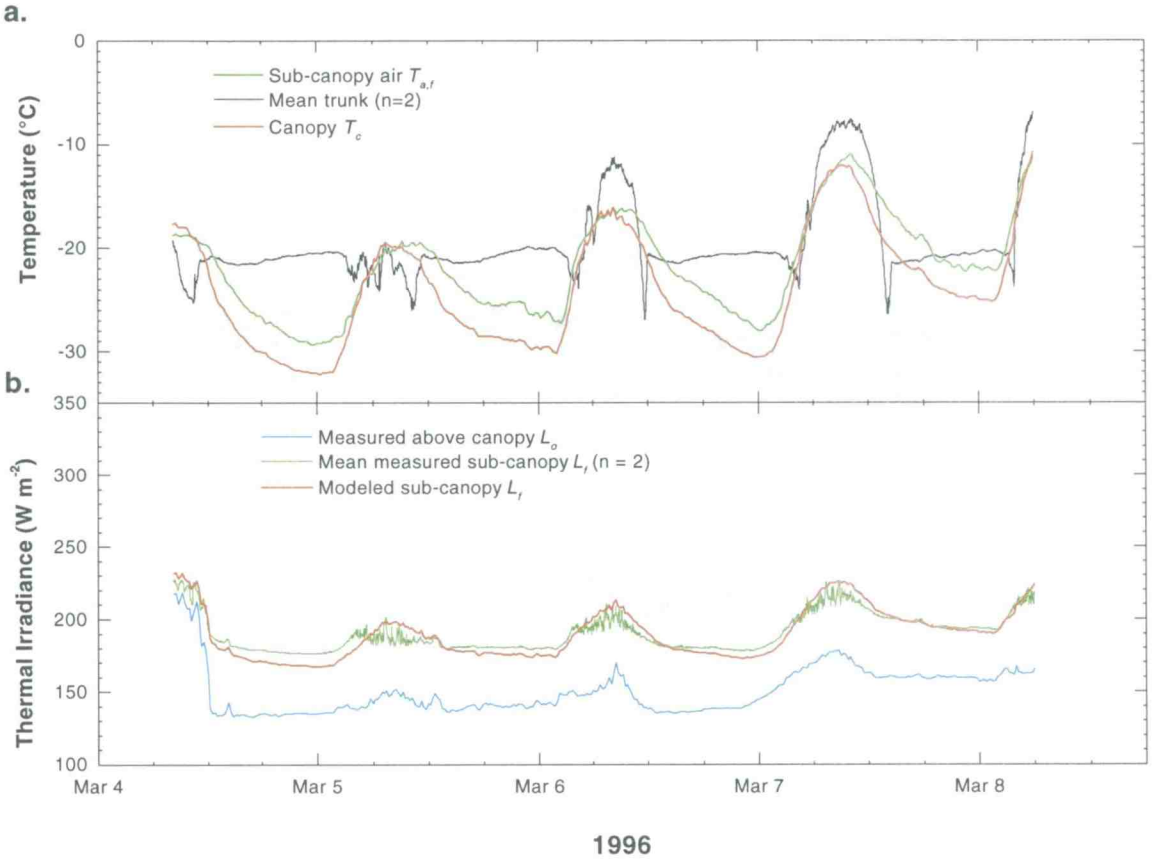

Figure 7. Temperatures and thermal radiation at the SSA OA site.

slightly underpredicting nighttime radiation, while slightly overpredicting daytime radiation, as shown by the modeled radiation trend in Figure 7b.

Wind Velocity

Wind velocities below the forest canopy (u_f), are typically lower than above-canopy wind velocities (u_o), due to sheltering effects of the forest canopies. Wind velocities control the snowcover turbulent energy fluxes, which are expected to comprise minor portions of the snowcover energy balance in the boreal environment (Hardy et al., 1998). Errors in below-canopy windspeed calculations should therefore have a negligible effect on the net snowcover energy balance. A very simple algorithm was used to estimate the below-canopy wind velocities, where all values are in m s^{-1}, and is written:

$$u_f = 0.2u_o \quad u_o > 1 \qquad [11]$$
$$u_f = 0.2 \quad u_o \leq 1.$$

The thresholding at low windspeeds was incorporated to ensure stability of the turbulent transfer routine in SNOBAL. Measured above- and below-canopy wind velocities, and calculated sub-canopy wind speeds during the 1994 IFC at the SSA-OJP site are shown in Figure 8, indicating general agreement between the calculated and measured time series.

Other Parameters

Sub-canopy air ($T_{a,f}$) and soil temperatures ($T_{g,f}$) are included in the standard suite of measurements taken by the SRC AMS, therefore, canopy adjustment algorithms were not developed for these parameters. Relative humidity (*rh*) measurements were only recorded above the forest canopies during the winter months. Below-canopy vapor pressures (e_a) were calculated by assuming constant *rh* profiles, and using $T_{a,f}$ to calculate e_a below the canopies. Although *rh* may be affected by the canopy, e_a during the winter

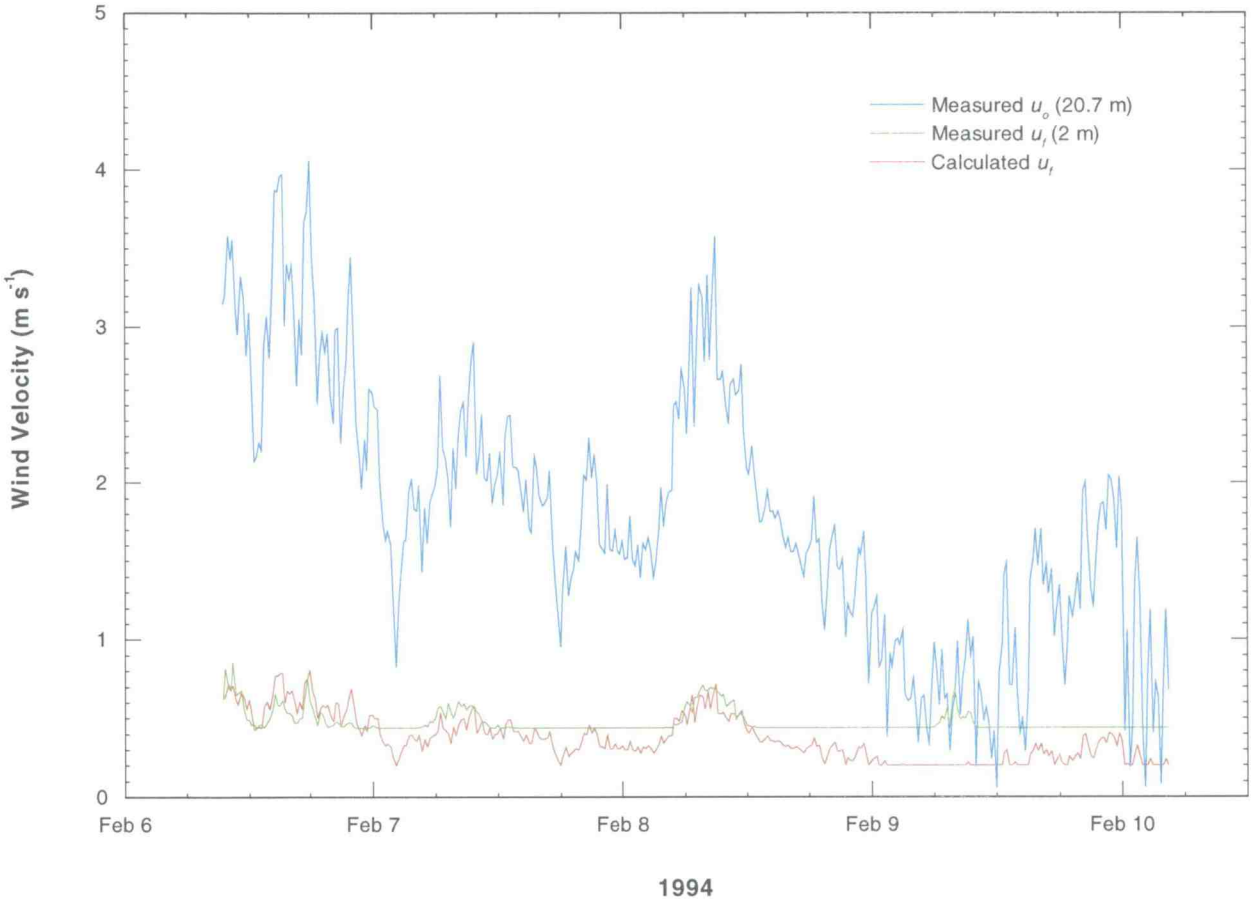

Figure 8. Above- and below-canopy wind speeds at the SSA OJP site.

and spring months is very low, such that calculated e_a values are not expected to be sensitive to small *rh* differences.

In many environments, interception of snowfall by forest canopies and subsequent sublimation may result in a significantly reduced snowpack in forested areas, relative to open areas (Meng et al., 1995; Stegman, 1996; Lundberg and Halldin, 1994). Observations of intercepted snow in the boreal environment indicate that almost all of the intercepted snow falls to the ground during periods of slight wind, or increased air temperatures (Sturm, 1992). The precipitation gauges were located in small canopy gaps; therefore we assume that the gauges effectively measure below-canopy precipitation, and that there is negligible loss of measured snow mass due to canopy interception.

Data Preprocessing

SNOBAL requires net snowcover solar radiation, incoming thermal radiation, vapor pressure, wind speed and air temperature near the snow surface, and soil temperature. Where sub-canopy data were not present, meteorological data were adjusted using the canopy adjustment algorithms. Where certain parameters were absent or anomalous at a given site, appropriate measures such as linear interpolation, and substitution of data from similar nearby sites were taken to provide reasonable and complete data records.

Meteorological Parameters

The snowpack net solar radiation is calculated at each timestep from $S_{d,o}$ and $S_{b,o}$ using the combined version of Equations [3], [6] and [7]:

$$S_n = (1-\alpha_d)(\tau_d S_{d,o} + \sigma_b S_{b,o}) + (1-\alpha_b)(S_{b,o} e^{-\mu h \sec(\theta)}) . \qquad [12]$$

τ_d and μ values were calculated at sites where sub-canopy solar radiation data were collected, and estimated based on canopy characteristics (e.g. conifer vs. deciduous) at

sites where no paired above- and below-canopy radiation data were collected. Values used for τ_d and μ are listed in Table 3. Incoming sub-canopy thermal radiation is calculated from L_o, τ_L, and T_c using Equation [10], except at the SSA-OA site where a canopy temperature adjustment was applied, as discussed above. Wind velocity is adjusted to account for canopy effects using Equation [11]. Sub-canopy vapor pressures are calculated using above-canopy *rh*, and sub-canopy T_a to account for humidity differences resulting from above- and below-canopy temperature variations. Sub-canopy soil temperatures are fixed at 0°C from the melt period forward in time to prevent anomalous modeled soil heat fluxes in the event of a simulated snowcover persisting beyond the actual snowcover. Sub-canopy air temperatures are used without modification.

Table 3. Canopy Parameters

Site	Cover Type	height (m)	τ_d, τ_L (dimensionless)	μ (m^{-1})
SSA				
OJP	Old Jack Pine	17	0.20	0.040
OA	Old Aspen	22	0.44	0.025
OBS	Old Black Spruce	10	0.16	0.074
NSA				
OJP	Old Jack Pine	13	0.20*	0.040*
YTH	Spruce / Poplar	13	0.30†	0.033†

Notes: *τ_d and μ assumed to be equivalent to SSA-OJP canopy cover
†τ_d and μ estimated to be intermediate between SSA-OJP and SSA-OA values

Precipitation properties are estimated from dewpoint temperature and precipitation records, according to the dewpoint temperature and density relationships listed in Table 4. Although SNOBAL is able to process mixed rain/snow events, mixed events are expected to comprise a minor portion of all precipitation events in the boreal

environment, therefore these simple relationships are used. Precipitation temperature is assumed to equal dewpoint temperature for all events.

Table 4. Estimated Precipitation Properties

Dewpoint Temperature Range(°C)	ρ_{pp} (kg/m^3)	Precipitation State
> 0.5	1000	rain
0.5 to 0.0	200	snow
0.0 to -5.0	100	snow
-5.0 to -10.0	75	snow
< -10.0	60	snow

Precipitation records were closely compared with the automated snow depth measurements, and were only corrected to the depth sensor where precipitation gauge readings appeared to be anomalous. This approach allows for the model inputs to be prepared almost exclusively from the precipitation record, thereby maintaining the integrity of the snow depth record as a model validation dataset. This approach also identified necessary adjustments to account for occasional undersampling of snow by the field instrumentation.

Site Specific Preprocessing

The AMS located at the NSA-YTH site did not include sensors for diffuse solar and thermal radiation. These parameters were therefore substituted from the NSA-OJP site located approximately 50 km to the west. As discussed above, an AMS was not located at the SSA-OBS site, therefore above-canopy data from the SSA-OJP site was used in conjunction with OBS canopy corrections for simulations at this site.

Anomalous soil temperature readings from the SSA-OA site suggest instrumental inaccuracies for the entire 1994-1995 winter season. Soil temperatures from the SSA-OJP site were substituted for all SSA-OA simulations. The soil heat conduction routine used by SNOBAL currently assumes a well drained mineral soil. Boreal soils tend to

have a thick layer of organic material and mosses overlying the mineral soil (Larsen, 1980), which effectively insulates the snowpack from the underlying soil. To account for the decreased thermal conductivity of organic-rich soils, the 10 cm soil temperatures were used instead of the default 50 cm soil temperatures to better approximate heat flow between the soil/snow interface.

Mass and Energy Balance Snowmelt Model (SNOBAL)

A detailed discussion of energy and mass transfer over a snow surface and development of SNOBAL was presented by Marks (1988), and is further discussed by Marks and Dozier (1992), Marks et al. (1992), and Marks et al., (in press). A complete description of the model, its input requirements, and output parameters is provided in Marks et al., (1998). SNOBAL was used without modification for all snowcover investigations presented here. An overview of the equations solved and model structure is presented to provide a basic description of the snowcover simulation approach.

Seasonal snowcover dynamics are controlled by temperature and vapor gradients within the snowcover, which are caused by energy exchanges at the snow surface, and at the snow-soil interface (Colbeck et al., 1979; Male and Granger, 1981). SNOBAL is driven by net snowcover solar radiation, incoming thermal radiation, air temperature, vapor pressure, wind speed, soil temperature, and precipitation mass, temperature, density, and state (solid/liquid) fraction. The model determines the snowcover depth, density and thermal properties from the meteorological conditions throughout the duration of the simulation. The model approximates the snowcover as being composed of two layers, a basal layer, and a fixed-thickness surface layer. At each time-step, the model computes the energy balance of each layer, and adjusts the thickness, thermal properties, and measurement heights of the forcing data accordingly.

The model calculates the energy balance of a snowcover at each time-step as:

$$\Delta Q = R_n + H + L_v E + G + M \qquad [13]$$

where:

ΔQ is the change in snowcover energy (W m^{-2}),
R_n is the net radiative energy flux (W m^{-2}),
H is the sensible energy flux (W m^{-2}),
L_vE is the latent energy flux (W m^{-2}),
G is the soil energy flux (W m^{-2}), and
M is the advected energy flux (W m^{-2}).

When the snowcover is in thermal equilibrium there is no change in the net snowcover energy (i.e. ΔQ=0). A positive change in snowcover energy will warm the snowpack, whereas a negative change in energy will cool the snowcover. Significant amounts of melt cannot occur until the entire snowcover reaches 0°C. When the entire snowpack is isothermal at 0°C, a positive energy balance will result in melt, and a negative energy balance will result in refreezing of any water contained within the snowpack. The model simulates each component of the energy balance, calculates the addition or depletion of mass by deposition, melt, evaporation, or runoff, and adjusts snowcover mass and thermal conditions at each time-step. Figure 9 provides a conceptual diagram of the model components.

Net radiation (R_n) is calculated as:

$$R_n = S_n + L - (\varepsilon_s \sigma T_s) \qquad [14]$$

where:

S_n is the net solar radiation (W m^{-2}),
L is the incoming thermal radiation (W m^{-2}),
ε_s is the snow surface emissivity (0.99, dimensionless)
σ is the Stefan-Boltzmann constant (5.6697 x 10-8 J m^{-2} K^{-4}), and
T_s is the temperature of the surface layer (°C), which is calculated by the model, and updated at the end of each time-step.

For the simulation of snowcover dynamics beneath the forest canopy, the net solar radiation S_n, is given by Equation [12], and the incoming thermal radiation is L_f, is given by Equation [10].

The general case of bulk energy transfer of sensible (H) and latent (L_vE) energy is described mathematically as:

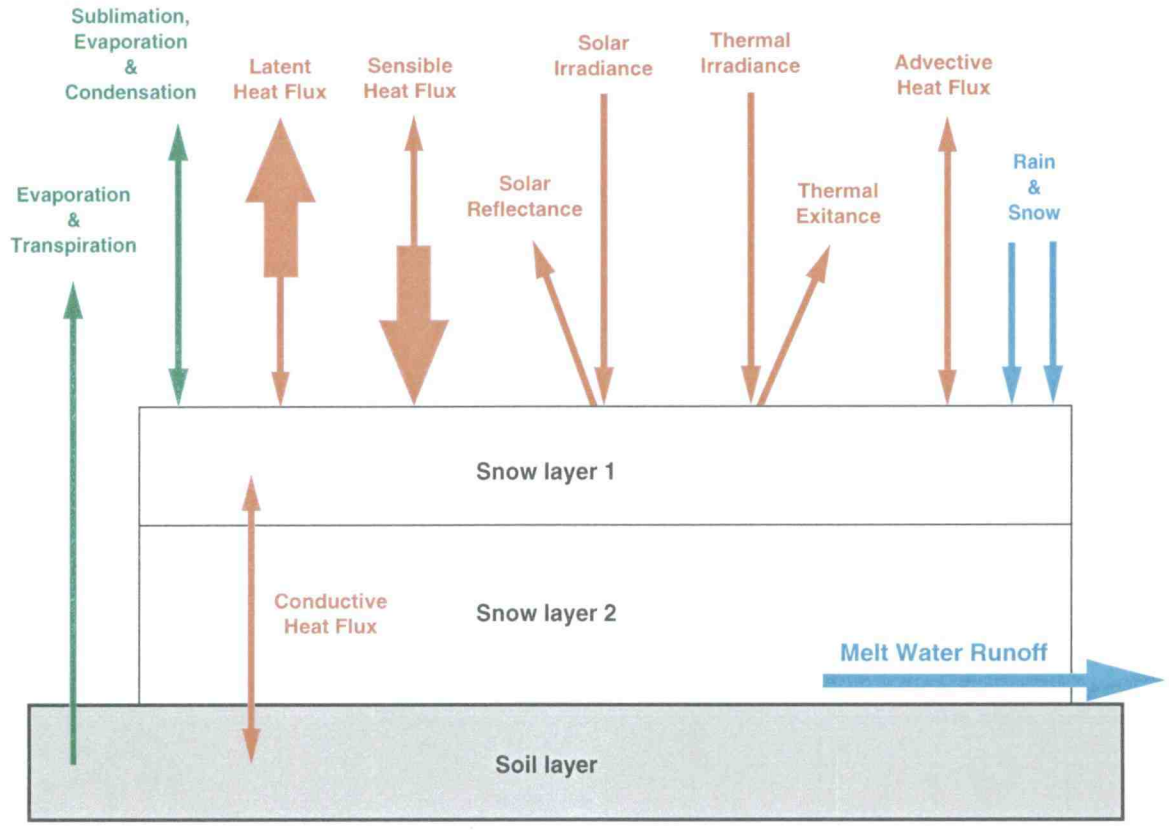

Figure 9. Conceptual diagram of the energy- and mass-balance components simulated by SNOBAL.

$$H = \rho_a C_p K_H (T_a - T_s) \quad [14]$$

$$L_v E = \rho_a K_W L_v (q - q_s) \quad [15]$$

where:

H is the sensible heat exchange (W m^{-2}),
E is the mass vapor flux (kg m^{-2} s^{-1}),
L_v is the latent heat of vaporization of water (2.5×10^6 J kg^{-1}),
ρ_a is the density of air (kg m^{-3}),
C_p is the specific heat of air (1005 J kg^{-1} K^{-1}),
K_H, K_W are the bulk transfer coefficients for heat and water vapor, respectively, and are strongly dependent on wind speed (J m^{-1} K^{-1} s^{-1}),
T_s, T_a are the potential temperatures of the snow surface and air, respectively (°C),
q_s, q are the specific humidity at the snow surface and in the air, respectively (Pa).

The turbulent transfer terms, H and $L_v E$ are calculated using a method adapted from Brutsaert (1982) by Marks and Dozier (1992) as a system of non-linear equations that

simultaneously solve for the sensible heat flux (H), and mass flux by evaporation or condensation from the snow surface (L_vE). Under most conditions, H is usually directed towards the snow surface, and is balanced by L_vE of similar magnitude away from the snowcover, hence the depiction of these fluxes as opposing arrows on Figure 9.

In general, energy transfer by conduction and diffusion between the soil and the snowcover (G) is calculated:

$$G = \frac{2K_{es}K_{eg}(T_g - T_s)}{K_{eg}z_s + K_{es}z_g} \quad [16]$$

where:

K_{es}, K_{eg} are the effective thermal conductivities for the snowcover and the soil, respectively,
z_g is the measurement depth (m) of the soil temperature,
T_g is the measured soil temperature (°C),
z_s is the thickness of the snowcover (m), calculated by the model, and
T_s is the temperature of the snowcover (°C), calculated by the model.

The model also calculates the energy transfer by conduction and diffusion between the upper and lower snowcover layers, using a similar formulation.

Advected energy (M) transfer to the surface snow layer, is only calculated during timesteps where precipitation occurs:

$$M = \frac{C_{p\_p}\rho_{pp}z_{pp}(T_{pp} - T_s)}{t_{step}} \quad [17]$$

where:

C_{p_p} is the specific heat of precipitation, calculated as a function of precipitation state (solid or liquid), temperature and density, estimated proportionally during mixed events,
ρ_{pp} is the precipitation density (kg m^{-3}),
z_{pp} is the depth of precipitation (m),
T_{pp} is the precipitation temperature (°C)
T_s is the snowcover temperature of the surface layer (°C), and
t_{step} is the length of the timestep (s).

Precipitation properties are all calculated as discussed above, and in Table 4.

The individual energy balance components are summed as indicated by Equation [13] to determine the energy available for melt or re-freezing in each of the snow layers. If melt occurs during a time-step, the model adjusts the thickness of the snowcover layers, snow density, liquid water content, and relative saturation. The specific mass of the snowcover is also adjusted by the total mass of evaporative loss, or condensation gain. If the total liquid water content exceeds the adjusted liquid water capacity, the excess becomes snowcover runoff, and snow density and specific mass are adjusted.

Results

Results of above- and below-canopy climate data analyses indicate that net snowcover solar radiation increases steeply in the spring months as a result of increased canopy penetration and snowcover absorption of solar radiation, and varies strongly as a function of canopy structure. In addition, net thermal radiation also increases during this period as a result of warmer air and canopy temperatures. Air temperatures, vapor pressures and windspeeds are very low during most of the snow season, and exhibit little variation between canopy types. The net snowcover energy balance is typically dominated by radiative fluxes, with minor contributions from turbulent and soil energy transfer. Net snowcover energy fluxes vary strongly with canopy type, primarily due to differences in radiative fluxes. Snowcover depth results indicate that simple canopy adjustment algorithms can be effectively used to estimate climate conditions beneath forest canopies for snowcover modeling investigations.

Climate Analyses

Observations of concurrent above- and below-canopy meteorological measurements illustrate the effect of the different canopy covers on the snow surface climate across the range of conditions encountered during an entire snow season. Analyses of above- and below-canopy climate differences improve our understanding of the processes controlling mass and energy transfer in forested systems.

Solar Radiation

Figure 10a depicts the seasonal solar and thermal radiation trends at the SSA-OJP site to illustrate the general trends observed at all sites. Figures 10b, c, and d illustrate the diurnal variations in radiation for five day periods ranging from low (~13°), mid

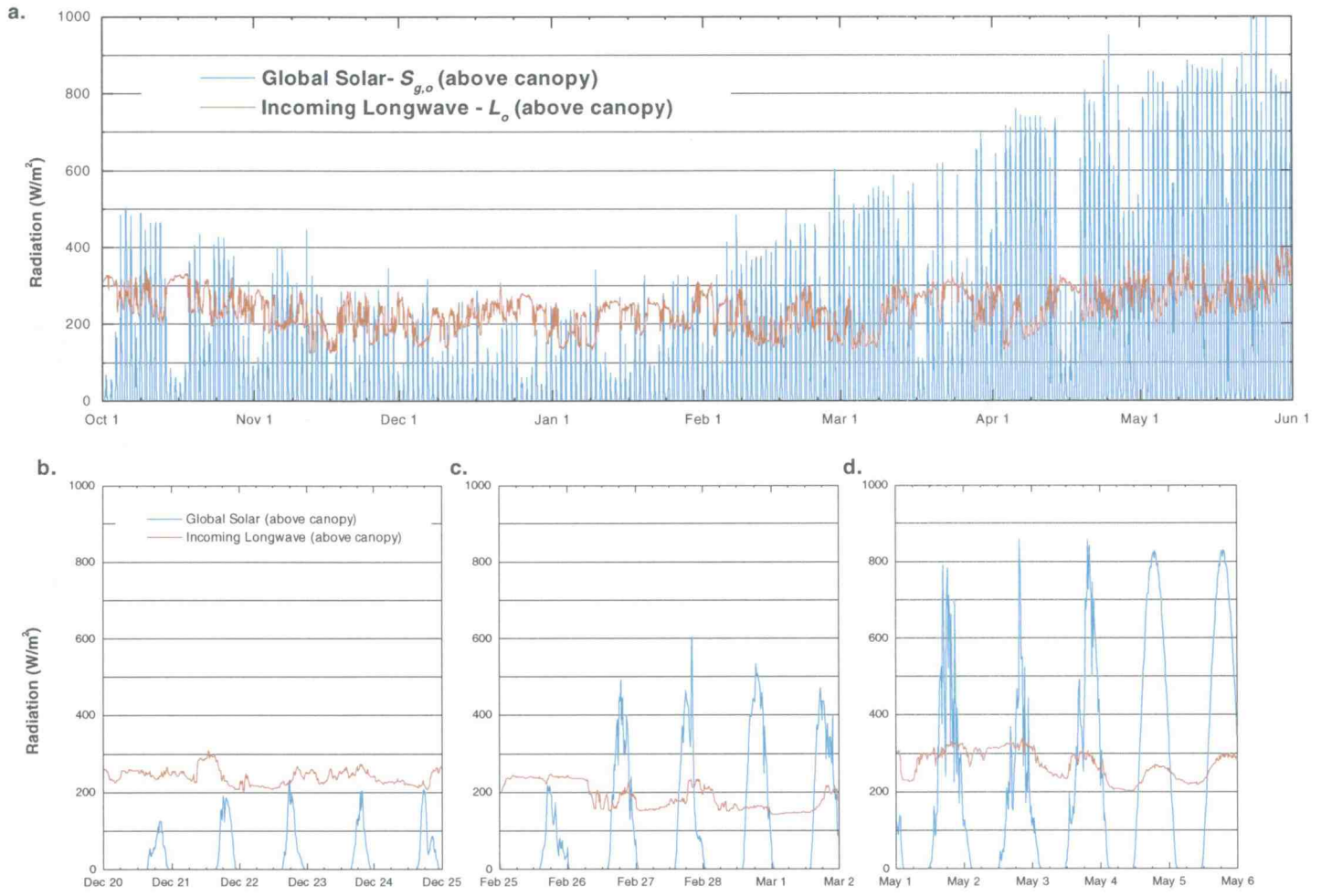

Figure 10. Above-canopy solar and thermal radiation at the SSA-OJP site.

(~28°), and high (~52°) maximum solar elevation angles. General seasonal and daily above-canopy solar radiation trends are illustrated by these figures, with slightly less radiation recorded at the NSA sites during most of the year. At the time when the permanent snowpack develops (~Nov. 1), clear sky radiation reaches a maximum of approximately 400 Wm^{-2} in both the NSA and SSA. At the lowest sun angles near the winter solstice, clear sky solar radiation decreases to a maximum of ~200 Wm^{-2} in the SSA, and ~100 Wm^{-2} in the NSA. During this time, days are approximately 6 hours long, resulting in very low daily shortwave energy fluxes. In early May, when the snowpack is actively melting, clear-sky noontime solar radiation values exceed 800 Wm^{-2} in both study areas. Solar energy flux is further maximized during this period by day lengths in excess of 15 hours, providing the dominant source of energy available for snowmelt over the diurnal cycle.

The calculated sub-canopy solar radiation ($S_{g,f}$) exhibits larger variation both between sites, and over the course of seasonal and diurnal cycles, due to forest canopy effects. Canopy-controlled radiation variations are illustrated in Figure 11, which depicts mean sub-canopy climate parameters for 2 week intervals over the course of the snow season. During the midwinter period (Dec. 1 - Feb. 1) mean solar radiation values are minimal, with values less than 20 Wm^{-2} beneath all canopies. The small mean radiation values occur due to strong radiation extinction by the canopies at the low solar elevation angles and short day lengths. Mean solar radiation beneath all canopies greatly increases during the late winter and early spring, as a combined result of increased transmittance through the canopy at higher sunangles and long days. During the period of maximum ablation rates, 2-week mean solar radiation values vary from approximately 90 to 200 Wm^{-2}, between the SSA-OBS and SSA-OA canopies, which represent the most optically dense (OBS) and most optically transparent (OA) canopy classes considered in these investigations. Mean sub-canopy radiation at the NSA-OJP sites exceeds the radiation at the SSA-OJP site as a result of increased canopy transmissivity due to the shorter canopy height. Similarly, the mean sub-canopy radiation at the SSA-OBS tends to be very similar to the SSA-OJP values because the shorter OBS canopy partially compensates for the lower optical transmissivity.

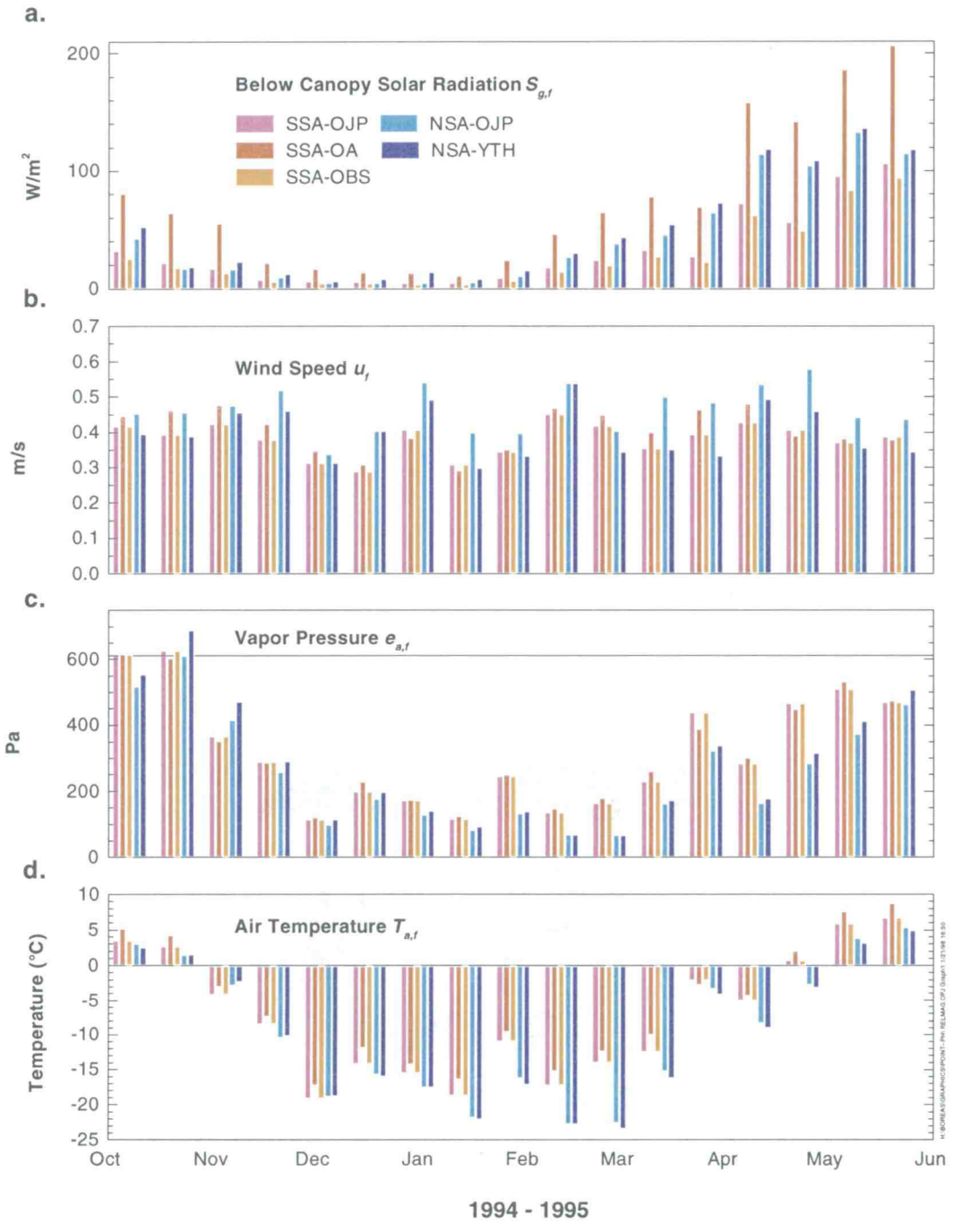

Figure 11. 2 week mean meteorological parameters.

Figure 12 illustrates the net snowcover solar radiation trend at the SSA-OJP site, calculated using Equation [12]. The net snowcover solar radiation is negligible during most of the winter months, as a result of low solar intensity, short day lengths, and very high snowcover albedoes, resulting from both clean snowcovers and low sunangles. The net radiation increases sharply in the spring months, as a result of higher intensities, longer days, and lower albedoes resulting from snowcover aging, debris deposition, and higher sun angles.

Thermal Radiation

Above-canopy thermal radiation shows little seasonal variation, increasing slightly in the spring months, relative to the winter months (Figure 10a). Above-canopy thermal radiation varies diurnally by about 50 Wm^{-2}, depending on local meteorological conditions, such as air temperature and degree of cloud cover. During the snow season, below-canopy thermal radiation is enhanced for all canopies by 13.5% on average, relative to above-canopy thermal radiation. The mean thermal radiation enhancement does not vary greatly between canopy types, ranging from approximately 11% for the relatively sparse Aspen canopy to 16% for the relatively dense Black Spruce canopy. Below-canopy diurnal variation is reduced relative to above-canopy conditions, and varies more regularly, as a result of canopy thermal inertia which tends to damp above-canopy thermal radiation cycles.

Net snowcover thermal radiation is also illustrated in Figure 12. The net thermal radiation was determined by the difference of the sub-canopy thermal radiation calculated using Equation [10], and of the thermal exitance of the snowcover, calculated using the modeled snow surface temperature in the Stefan-Boltzmann equation. Figures 12a, b and c indicate that during the winter months, net daytime thermal radiation frequently exceeds net solar radiation. During the spring months, thermal radiation comprises a smaller portion of the radiation balance, as indicated in Figure 12d. Daytime snowcover thermal absorption is commonly equaled or exceeded by nighttime thermal emission, resulting in a net radiative loss of energy when integrated over time.

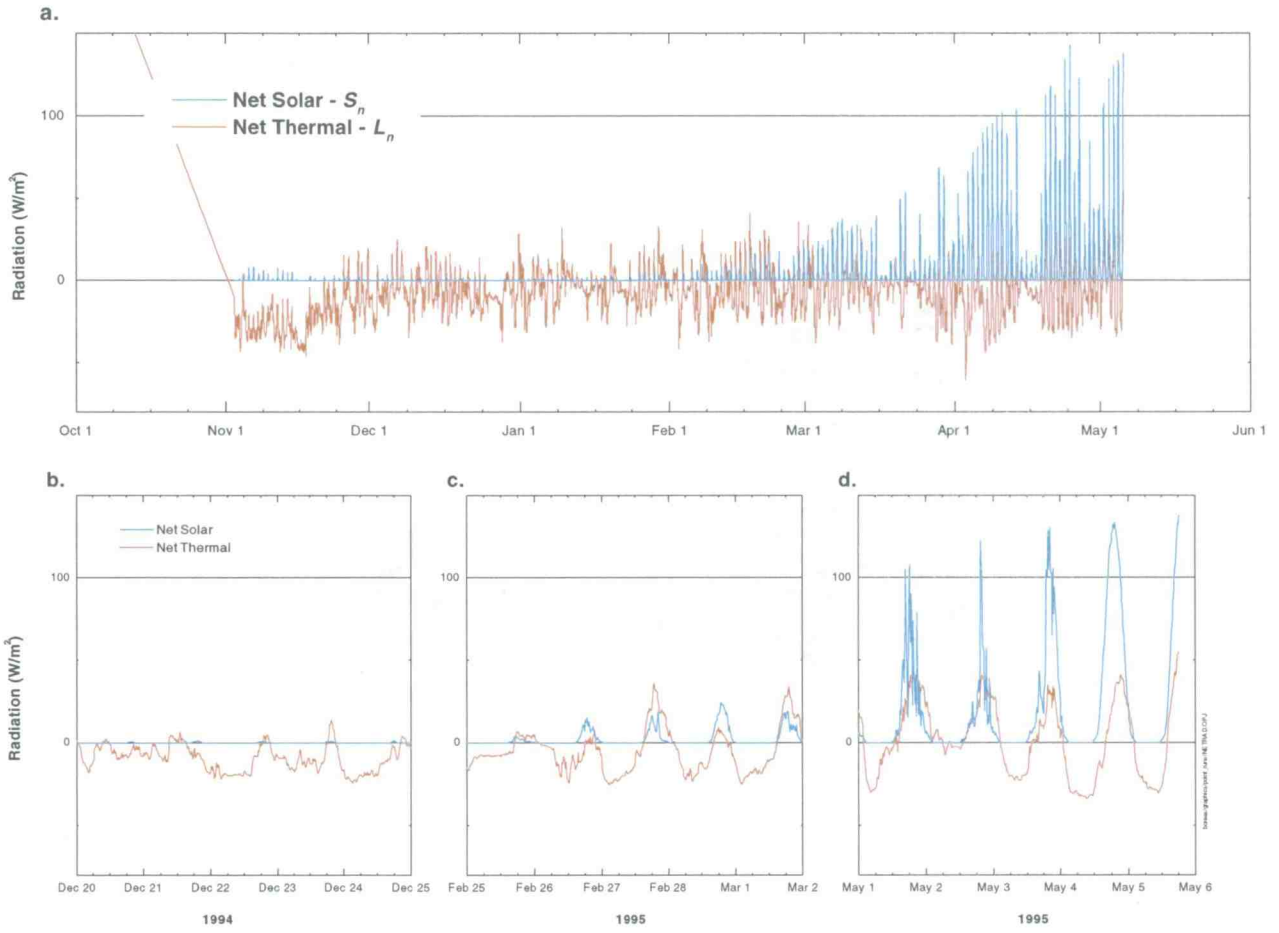

Figure 12. Calculated net snowcover solar and thermal radiation at the SSA-OJP site.

Within Canopy Air and Canopy Temperatures

Within canopy air temperature trends for the 1994-1995 snow season at the SSA-OJP site are illustrated in Figure 13a. Variations between above-canopy air, within-canopy air, and canopy surface temperatures for three periods during the snow season are shown in Figures 13b-d. Within canopy air temperatures during the 1994-1995 winter season at the SSA remained below 0°C from November through mid-March, with several exceptions. The period from March through complete ablation in early May is characterized by above freezing daytime temperatures, and consistently below freezing nocturnal temperatures, interspersed with extended periods of below 0°C temperatures. Within canopy air temperatures are consistently cooler than above-canopy air temperatures, particularly at night, during most of the snow season.

Within canopy temperatures at the NSA were much cooler than at the SSA, remaining below -10°C for most of the period from mid-November through early March. Temperature variations from early March through complete ablation, are similar to the SSA sites, with above freezing daytime temperatures, and sub-freezing nocturnal temperatures.

Canopy temperatures at the SSA-OJP site are elevated relative to within canopy temperatures by about 2-3 °C, during most of the snow season (Figures 13b & c). During the spring months, the temperature differences increase in magnitude, and can exceed 5 °C during the daytime, as a result of increased incident solar radiation. Canopy temperature fluctuations and differences are greatest during clear sky conditions, when radiant heating and cooling of the forest canopy is most efficient. During overcast conditions, air and canopy temperatures approach equality, with small diurnal fluctuations. In general, canopy and air temperature relationships are similar at the NSA sites, however the differences between the two temperatures tend to be much smaller during the entire snow season.

Mean 2-week air temperature differences between sites are shown in Figure 11. Within canopy temperatures at the SSA-OA site tend to be slightly warmer during most of the snow season. Temperatures within both NSA canopy covers are very similar, and

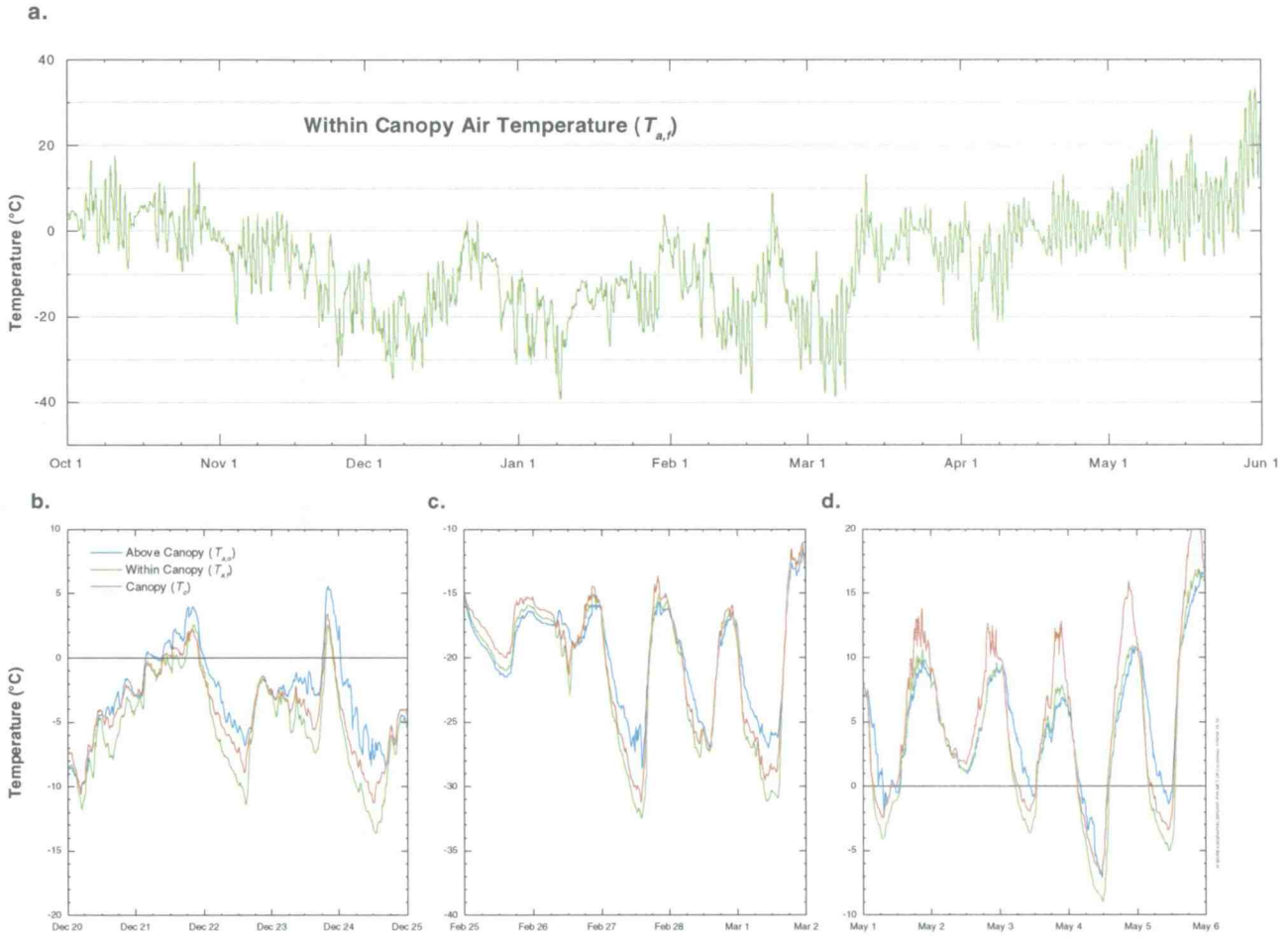

Figure 13. Temperature measurements at the SSA-OJP site.

are consistently colder than the SSA sites. SSA-OJP and SSA-OBS within canopy air temperatures are assumed to be equal, as discussed above.

Other Forcing Parameters

Vapor pressure measurements during the snow season are very low, as expected for extremely cold environments. Vapor pressures during spring melt at the SSA oscillate above and below 611 Pa (saturation vapor pressure at 0°C), and gradually increase over time. This indicates that during the ablation period, the direction of the vapor pressure gradient between the air and snow surface (and therefore potential latent heat flux) oscillates, while becoming increasingly positive over time. At the NSA sites however, vapor pressures remain below 611 Pa for almost the entire ablation period, indicating a vapor gradient directed away from the snow surface. In such an environment, the snowcover is expected to lose mass and energy by evaporation, thereby cooling the snowcover. Mean vapor pressure differences between sites appear to be due to air temperature differences between the sites (Figure 11).

Fifteen minute mean above-canopy wind velocity measurements are observed to be high during most of the model simulation periods, frequently exceeding 5 m/s. The application of canopy and thresholding adjustments reduces the below-canopy wind velocities to between 0.2 and 1.0 m/s. Mean wind velocities are relatively stable throughout the snow season, with slightly higher velocities occurring at the northern sites (Figure 11).

SSA-OJP soil temperatures at 10 cm exhibit strong diurnal fluctuations in the autumn months, until the first major snow event occurs. Following the first major event, soil temperatures steadily decrease to 0°C over approximately 3 weeks. After freezing, soil temperatures continue to decrease, eventually reaching an annual minimum temperature slightly less than -7°C. Soil temperatures increase to 0°C through the late winter and spring months, reaching and maintaining a temperature of 0°C for roughly 2 weeks, as the soil thaws, and 0°C meltwater infiltrates through the soil profile. Soil temperatures at the NSA-OJP site freeze slightly earlier than at the SSA-OJP site, and decrease to a minimum of -14°C during midwinter. During soil warming, 0°C conditions

at the NSA-OJP site are maintained for a period of approximately 1 week. 10 cm soils at the NSA-YTH site freeze at the same time as the NSA-OJP soils, but only reach a minimum temperature of -5°C. Soils at NSA-YTH warm to 0°C approximately 1 week sooner than the OJP site, but maintain 0°C conditions for 2 weeks.

Snowcover Energy and Mass Balance Simulations

SNOBAL was run at a 15 minute time-step from October 1, 1994 through June 1, 1995, using canopy-corrected meteorological data at the OJP, OA, and OBS sites in the SSA, and at the OJP and YTH sites in the NSA. Model results are validated using automatic and manual snow depth measurements from the various canopy covers. Results from the seasonal snowcover simulations serve to quantitatively describe the processes of snowcover mass and energy transfer beneath variable canopies in the boreal environment for an entire snow season, and to provide a means to evaluate the performance of simple canopy adjustment algorithms.

Snowcover Energy Balance

Figures 14a-f present the 15-minute average values for ΔQ, R_n, G, H, L_vE and, M for the SSA-OJP site, to illustrate snowcover energy flux trends beneath a moderately transmissive canopy. Figure 15 presents the relative contribution of the net all-wave radiation (R_n), soil heat (G), advected (M), and sum of the sensible and latent heat fluxes ($H + L_vE$) to the total snowcover energy flux (ΔQ), at all sub-canopy sites.

The sum of the energy balance terms (ΔQ) oscillates during the snow season, and is typically positive during the day and negative during the night (Figure 14a.). From the deposition of a permanent snowcover in November, through February, the 2-week mean monthly net snowcover energy remains at or near zero for all sites. From March through complete snowcover ablation early May, the mean net energy is consistently positive, and increases steeply at all sites.

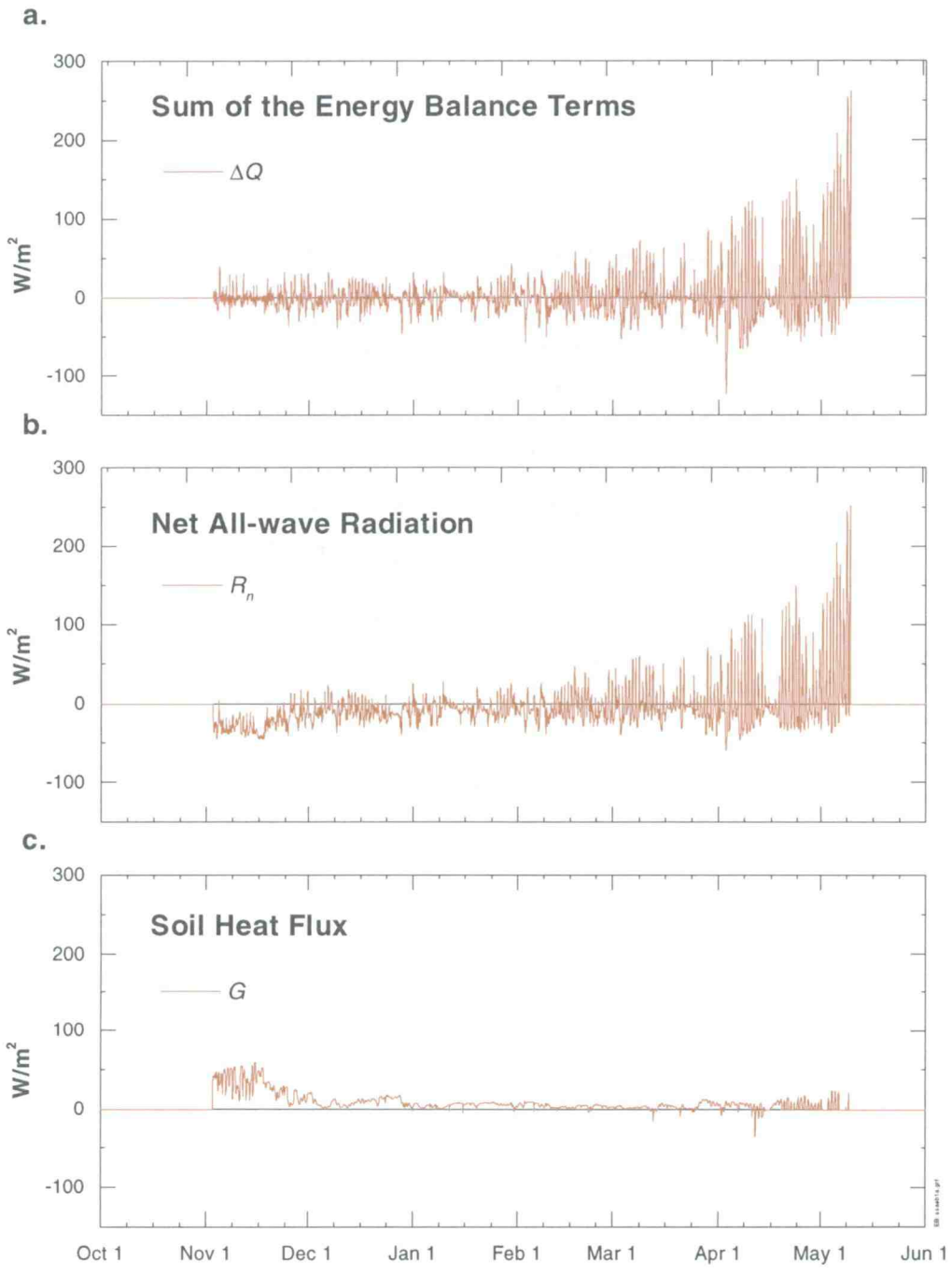

Figure 14. Simulated snowcover energy-balance trend, SSA-OJP site.

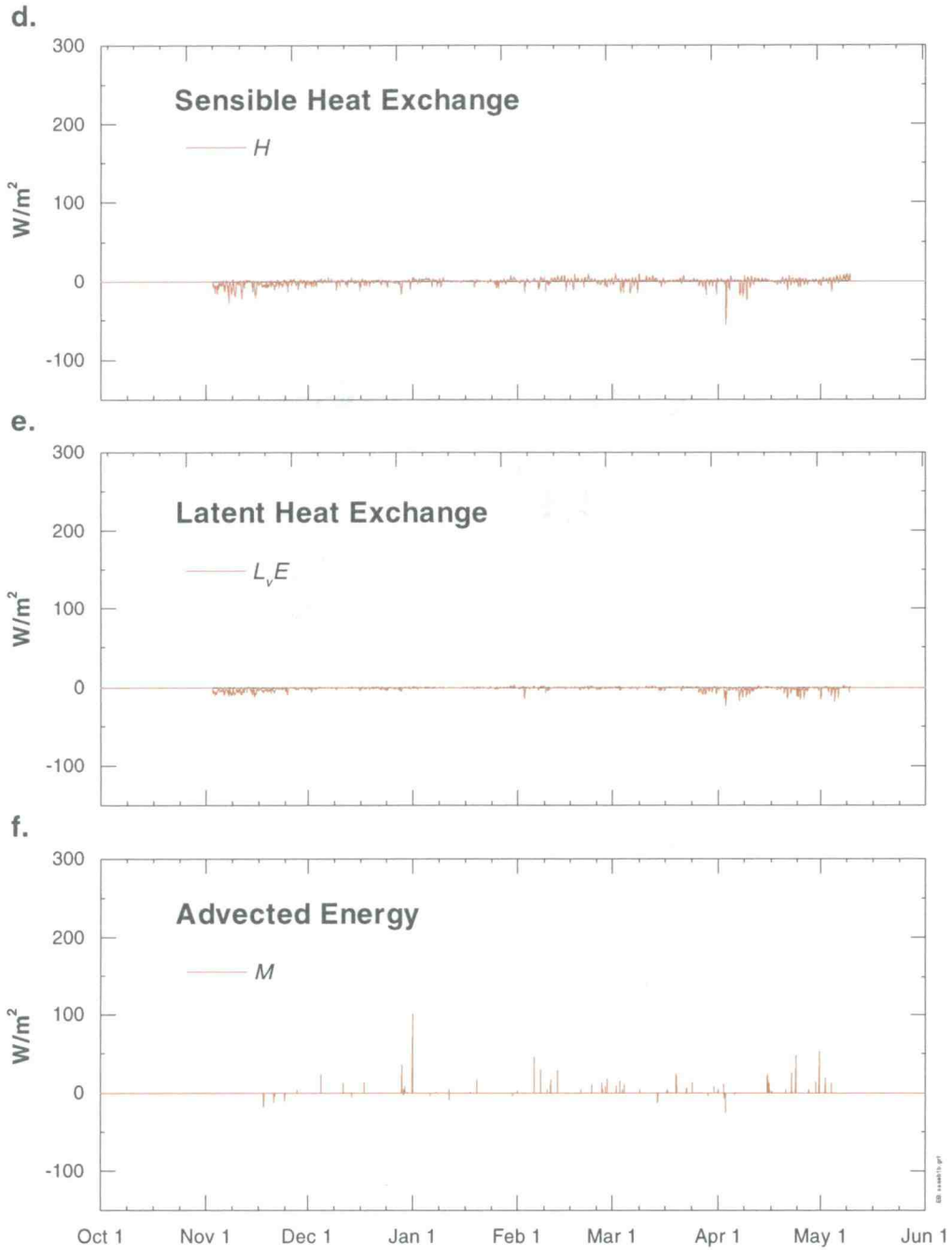

Figure 14. (continued).

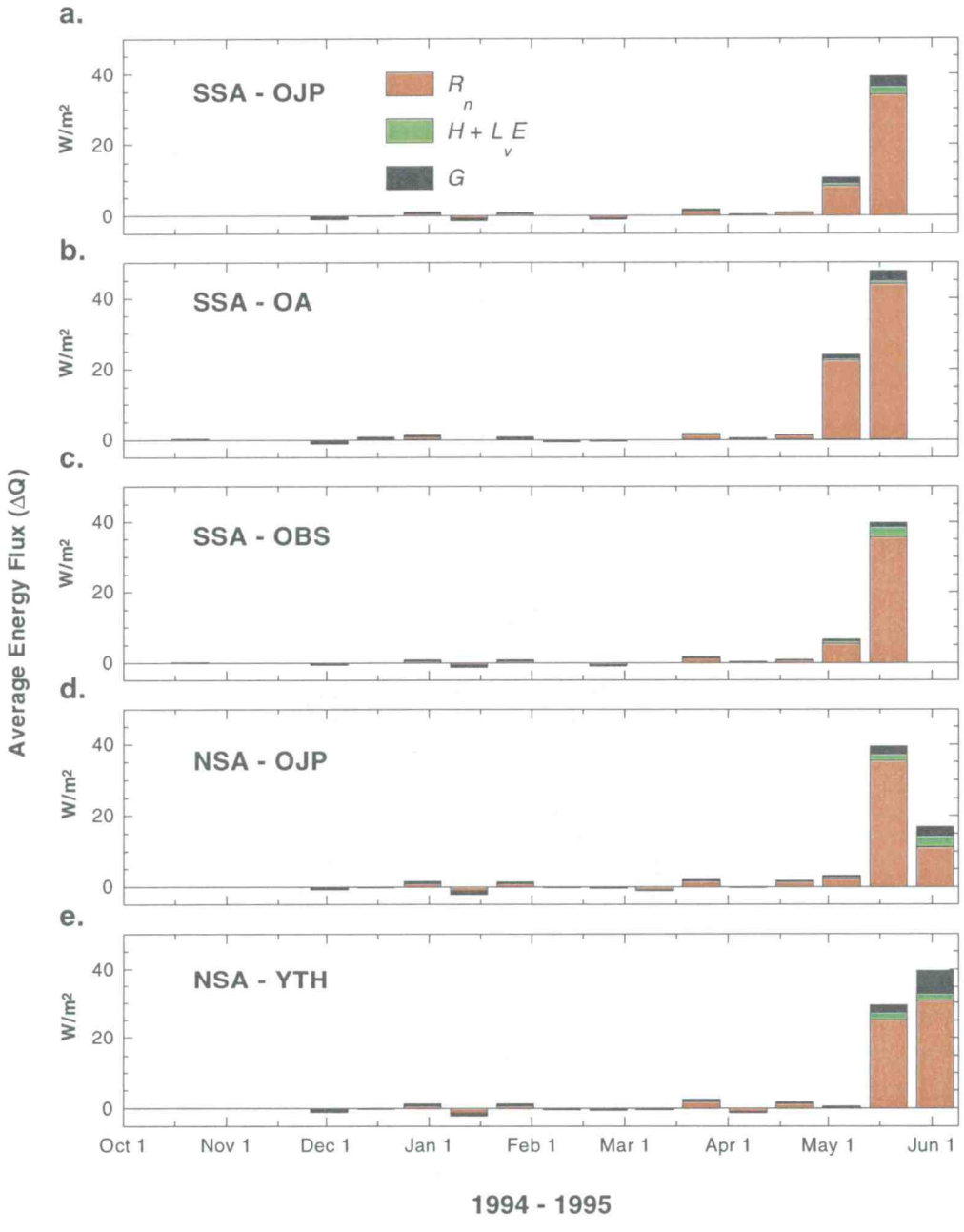

Figure 15. 2-week relative snowcover energy fluxes.

During the autumn and winter months, the net snowcover radiation trend (R_n) is slightly negative, and closely mirrors the net thermal radiation, indicating radiative cooling of the snowcover (Figure 14b.). During the spring months, R_n more closely mirrors the net solar radiation trend, becoming increasingly positive during the day, but remaining slightly negative during the night. During the entire snow season, R_n typically dominates ΔQ at all sub-canopy locations in the BOREAS study region as indicated in Figure 15. The primary difference between sites is in the variation of R_n contribution, which is larger in the transmissive canopies and smaller in the optically dense canopies.

Soil heat flux (G) comprises a major portion of the energy balance early in the snow season while the soil releases energy as it cools and freezes (Figure 14c.). Soil heat flux is slightly positive throughout most of the snow season, increasing slightly during the spring meltout. Although the relative contribution of G to the total energy flux is large early in the season, the mean ΔQ is very small during this time, as indicated in Figure 15.

The net turbulent energy transfer ($H + L_vE$) comprises a minor portion of the energy balance at all sites (Figure 15). Sensible heat fluxes (H) oscillate in direction during the snow season, whereas latent heat fluxes (L_vE) tend to be negative throughout the season, indicating evaporative cooling of the snowcover (Figure 14d. and e.). Beneath the conifer, and mixed canopies, H and L_vE tend to both be slightly negative during most of the snow season due to extremely low air temperatures and vapor pressures. H within the OA canopy remains slightly positive during the course of the snow season, due to higher air temperatures, while latent exchanges are negligible throughout the winter.

Advective energy transfer tends to be sporadic and positive during the winter months, as warmer snow is deposited on top of a cold snowpack during occasional precipitation events. (Figure 14f.) During spring meltout, small positive advective fluxes occur during several rain events. Advected energy fluxes are negligible, when averaged over 2 week periods, and are therefore not included in Figure 15.

Snowcover Mass Balance

When snow is present, SNOBAL calculates runoff as the sum of melt, less the available liquid holding capacity of the snowcover, plus rain. Early in the spring, several minor melt events that do not exceed the water holding capacity of the snowcover occur at all sites. The production of runoff at all sites follows a distinctly diurnal trend driven by net radiation variability, with irregular runoff spikes resulting from isolated cold (~0°C) rain events.

At the SSA sites, melt with associated runoff production starts at approximately April 16 and continues over a period of 3 weeks at the three sites, with both sites exhibiting complete ablation by approximately May 7. Maximum sustained melt rates beneath the Aspen canopy exceeded 1 mm/hr, whereas maximum sustained melt rates beneath the OJP and OBS canopies approached 0.7 mm/hr. The variation in melt rates, coupled with a larger snowpack beneath the OA canopy resulted in synchronous complete ablation observed both with the model results and with empirical measurements.

The onset of spring meltout at the NSA sites occurs at close to the same time as at the SSA sites. Snowpack masses are very similar at both the SSA-OJP and NSA-OJP sites, however, slower melt rates in the NSA-OJP result in complete ablation 2-3 days later than at the SSA-OJP site. Melt rates at the NSA-YTH site are comparable to the NSA-OJP site, however a substantially larger snowpack results in an extended ablation period, with complete ablation occurring almost 1 week after the NSA-OJP site.

Model Validation

Continuous automatic depth measurements from small open areas within each canopy are used to validate the simulated snowcover depths. In addition, mean depth measurements recorded manually during bi-monthly snow course surveys within each canopy type are used to provide an additional validation dataset. Snow course measurements are not located in close vicinity to the sites where AMSs are located, but were chosen to be representative of conditions beneath the various land cover types. The

manual snow course measurements are useful to validate the SNOBAL results and to evaluate the performance of the canopy adjustment algorithms at other forested sites where detailed sub-canopy meteorological measurements are absent.

Figures 16a-e show the automatic and manual measured and modeled snow depths for the SSA-OJP, SSA-OA, SSA-OBS, NSA-OJP, and NSA-YTH sites. No AMS was installed at the SSA-OBS site, therefore the manual snow course data for a black spruce canopy 43 km to the southeast is used to evaluate data preprocessing and model performance at this site. The simulated snow depths closely match the automated snow depth measurements over the entire snow season at all sites. The simulated snowpack completely ablates from 5 to 6 days later than the measured ablation at the three SSA sites. Modeled depths also agree closely with the manual measurements, and appear to more closely match the observed meltout dates.

Modeled ablation dates occur approximately 2 days later than measured dates at the NSA sites. The modeled depths beneath the OJP canopy agree very closely to the measured depths, indicating that the preprocessing algorithm developed at the SSA-OJP site can be effectively applied to the NSA-OJP site. The measured and modeled depths for the NSA-YTH site exhibit the most divergence of any of the sites, apparently related to an early-season melt event, that caused substantial compaction of the snow cover. This divergence may be due to inaccurate assumptions which were made with regards to the nature of the forest canopy at this site. It is important to note however, that given limited knowledge of the canopy characteristics, close agreement between the two depth traces was obtained, accurately simulating the ablation delay at this site relative to the OJP site.

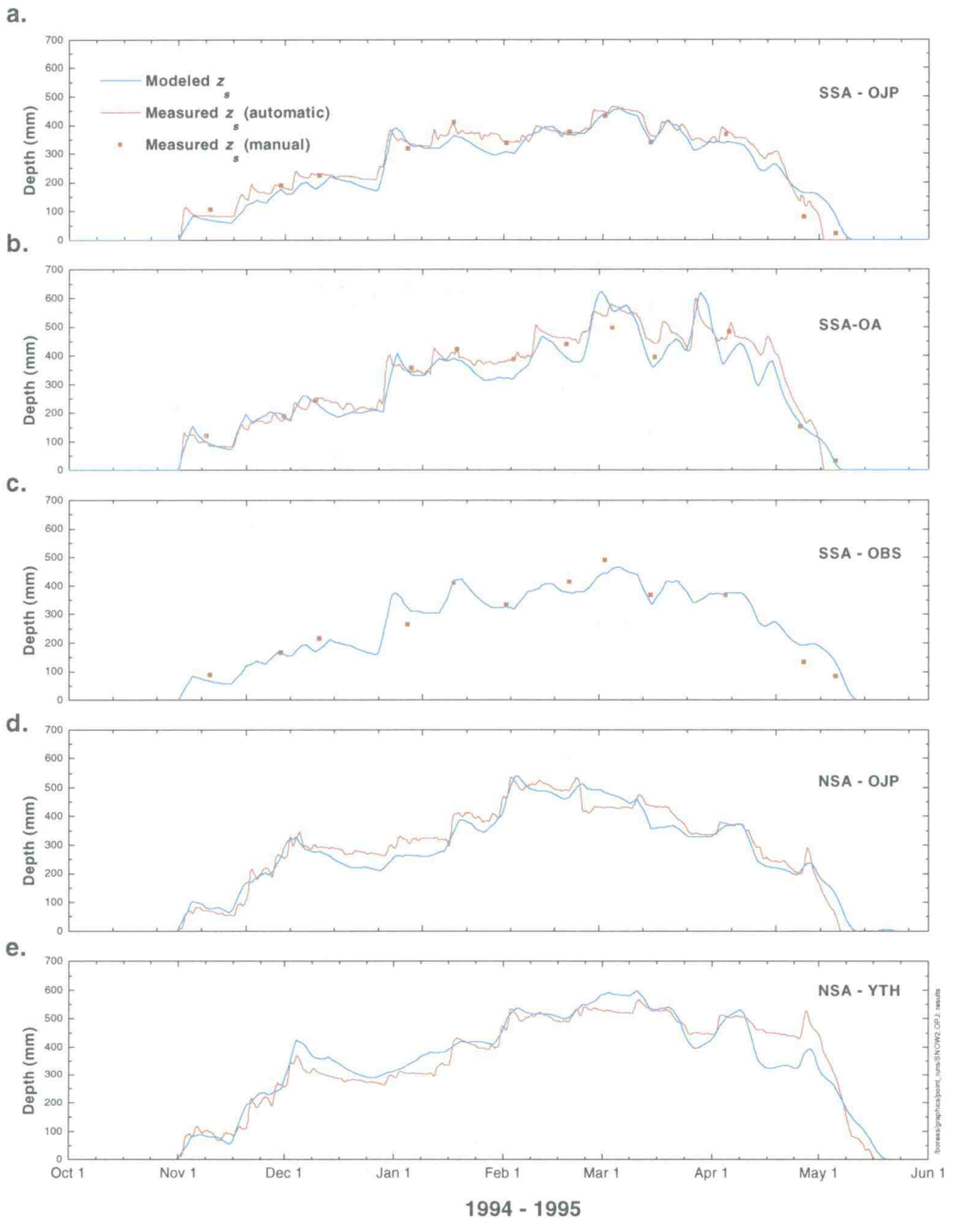

Figure 16. Measured and simulated snow depths.

Discussion

Results of the SNOBAL simulations clearly indicate that on average, the snowcover energy balance within the boreal forest is either negative or close to zero for the winter months, becoming increasingly positive throughout the spring (Figure 15). The springtime energy gain is dominated by net radiation fluxes with negligible contributions from turbulent, soil heat and advected energy fluxes. This suggests that relatively large errors in calculated turbulent, soil heat and advected energy may not adversely affect the simulated snowcover results. Highly accurate canopy adjustment algorithms for wind speed, vapor pressure, and air temperature are probably not essential to accurately simulate snowcover deposition and ablation beneath boreal forest canopies, given the minor turbulent flux components. Simple adjustments for sub-canopy wind speed reductions, and the assumption that relative humidities beneath the forest canopy are equivalent to above-canopy relative humidities, are therefore acceptable for modeling sub-canopy snowcover dynamics. Analyses of above- and below-canopy air temperatures indicate that the sub-canopy air temperature is usually colder than the above-canopy air temperature. Other investigations concerning sites where sub-canopy air temperatures are not measured should consider the potential alteration of canopy covers on surface climate conditions.

The minor contribution of soil heat flux during the winter and spring (Figure 15) suggests that the thermal characteristics of soils need not be considered in great detail for studies focusing on just the spring meltout. The larger soil heat flux contribution observed early in the snow season indicates that the thermal characteristics of boreal soils must be considered in detail for snowcover simulations containing the period of snowcover development. These investigations identified that the inherent SNOBAL assumption of a well-drained mineral soil is not applicable to all sites in the boreal regions, probably due to the presence of organic materials in the soil profile. The lower rate of heat conduction within boreal soils can be accounted for by using relatively shallow soil temperature measurements to provide a more accurate estimate of

temperatures at the base of the snowpack. SNOBAL could be improved by including parameters identifying basic soil characteristics of a site, in order to more accurately calculate soil heat fluxes. Such improvements are only necessary for investigations which include the development of a seasonal snowcover, or the periodic deposition and ablation of transient snowcovers.

The relative importance of radiation in this environment, where the forest canopy acts as the primary control on radiation at the snow surface (Figure 15) indicates the necessity of accurate canopy adjustment algorithms for solar and thermal radiation. Adjustment algorithms which can be driven with forest parameters easily derived from GIS or remote sensing products are therefore necessary to complete spatially distributed snowcover model runs in the boreal environment. The five snowcover simulations indicate that simple cover class and zenith angle-dependent correction factors can be applied to open site radiation data to describe radiation regimes beneath forest canopies for snow cover modeling, assuming homogeneous covers.

The close agreement between the measured and simulated snow depths (Figure 16) in canopies where no sub-canopy radiation measurements were completed (i.e. NSA-OJP, NSA-YTH, and sub-canopy snow course locations) suggests that canopy optical parameters may be estimated from limited knowledge of canopy cover classification and height. Radiation transfer theory suggests that the canopy structure parameters (μ, τ_d) may not need to be known with a high degree of accuracy, since canopies modulate the radiative input by re-emitting absorbed solar radiation as thermal radiation. Errors in the transmitted solar radiation will therefore be partially compensated by opposing errors in thermal emission, reducing the sensitivity of the calculated below-canopy radiation to the canopy parameters.

The radiation adjustment algorithms used in these simulations are effective at the 5 relatively homogeneous sites, however, these techniques may not be adequate for rigorous spatially distributed snowcover modeling, requiring a high degree of accuracy for all land cover classes. Geometric optical radiative transfer studies of conifer canopies clearly indicate that simple Beers-Bouger-Lambert Law adjustments to open site radiation data, do not accurately describe the transfer of solar radiation beneath sparse,

short, or highly discontinuous canopies (Ni et al., 1997). More accurate adjustment algorithms for solar radiation should therefore be driven by a minimum of species type, height, stem density, and crown dimensions, to accurately describe radiation beneath highly variable canopy types. Application of the general techniques developed for radiation adjustments in forests by Price (1997), will provide more accurate distributed radiation fields beneath highly variable canopies.

The adjustments for solar radiation include a series of simplifying assumptions that may be corrected or improved. The adjustments used in these investigations assumed the canopy to be an isotropic absorber, with μ constant at all sun angles. Empirical and modeling studies indicate that a greater proportion of radiation is transmitted at relatively low sun angles than would be predicted if the canopy were to act as an isotropic absorber, due to the horizontal orientation of the branch elements (Ni et al., 1997, Pomeroy and Dion, 1996). The adjustments used in these simulations are therefore expected to underestimate sub-canopy solar radiation at low solar elevation angles. Validation data suggest that this underestimation may not significantly affect the simulated snowcover dynamics at the five sites. This is because low incident solar energy and high snow albedoes at low sunangles render canopy transmission errors insignificant. Conversely, the canopy transmittance parameters were derived from mid-winter measurements, and may inherently account for increased transmittance at low sunangles, potentially causing transmittance at high sun angles to be overestimated.

Snowcover radiative energy transfer in forested systems is also affected by the spectral properties of the incoming radiation and canopy elements. Conifer canopies strongly absorb radiation in the visible portion of the electromagnetic spectrum, while preferentially reflecting and transmitting near infrared (NIR) radiation. NIR radiation may also be enhanced at low solar elevation angles typical of the high latitude boreal environment. The near infrared snowcover albedo is less than the visible snowcover albedo. The adjustment algorithms do not account for the spectral alteration and increased absorption of radiant energy in the near infrared portion of the electromagnetic spectrum. The omission of canopy spectral properties in the adjustment algorithms may therefore result in the underestimation of snowcover net solar radiation.

Measured and simulated snow depth values suggest that systematic or significant adjustment inaccuracies discussed above may be negligible. Underestimates of net solar radiation due to spectral characteristics of the canopy and snowcover may cancel overestimates of transmitted radiation. Similarly, any potential errors in sub-canopy radiation may be compensated by estimated variations in the snowcover albedo resulting from debris deposition. It is important to note however, that any errors in the individual radiation components should not siginificantly affect the overall energy and mass balance analysis of the seasonal snowcover, due to the dominance of net radiation in this system.

The simulated snowcover at all five sites completely ablates from 1 to 6 days later than the observed ablation dates, consistent with SNTHERM simulations at the SSA-OJP site (Hardy et al., 1997). The discrepancies in the results presented here may be due to inaccuracies in the canopy adjustment algorithms or approximate debris deposition functions. The snowcover albedo calculations also neglect the albedo decrease resulting from the solar radiation penetration of very shallow snowcovers, which may delay simulated melt. The calculation of turbulent energy exchange assumes a continuous snowcover, which may not be present prior to complete ablation at a given point. Violation of this assumption is likely to slow the simulated snowmelt, due to the inability of the turbulent transfer routines to simulate small scale advection of warm, relatively humid air masses from patches of bare ground (Shook and Gray, 1997).

Ablation dates for the three SSA sites were very similar despite differing canopy structures. The differences between sites are reduced due to a greater quantity of SWE and taller canopy at the OA site, and a relatively short OBS canopy, which partially offsets the lower optical transmissivity of the denser canopy. The northern and southern OJP sites also ablate at approximately the same time, apparently due to shorter canopy heights in the NSA, which permit greater transmittance of solar radiation, relative to the taller SSA-OJP canopy. Complete ablation is delayed at the NSA-YTH site, despite larger canopy transmissivity values due to greater amounts of SWE deposited at this site. Comparisons between the various sites and canopy covers illustrates how both depositional patterns and variations in canopy structures interact to control the rate and volume of melt water delivery to a given site.

The results suggest that snowcover ablation in the boreal forest may be more sensitive to shifts in land cover patterns, which strongly affect snowcover radiative fluxes, rather than more subtle climate changes which may affect the relatively minor turbulent fluxes. In general, land cover changes toward more open and deciduous canopies will increase the rate of snowmelt delivery, and advance the date of complete ablation. Predicted climate shifts toward drier conditions may similarly advance the date of complete ablation, due to reduced total snowcover and sunnier conditions. Advances in snowcover ablation dates will consequently advance and extend the seasonal warming and drying of the boreal regions. Hydrologic and energy-balance studies of the boreal regions must therefore consider expected changes in both land-use and depositional patterns, due to the strong role each exerts in controlling seasonal changes in the surface energy balance of a region.

The dominance of the radiative energy component of the snowcover energy balance beneath forest canopies illustrates the importance of high quality above- and below-canopy radiation measurements, both to develop quantitative descriptions of forest canopies and to drive energy balance snowcover models for hydrological analyses. To fully characterize the radiative transfer processes within forest canopies, detailed above-canopy global solar, diffuse solar, and thermal measurements should be taken over a minimum of 1 annual cycle. These measurements should be coupled with below-canopy global and thermal radiation measurements at several times during the year, to analyze transfer processes at a full range of sun angles and canopy conditions. The addition of forest element (e.g. canopy, branch, trunk) surface temperatures can provide valuable information regarding the thermal radiative characteristics of canopies. Detailed radiation measurements within and above a variety of canopy types as in the BOREAS investigation, yields valuable information which improves the understanding of energy transfer processes for hydrologic investigations, and assists in the analysis of the potential effects of changing land cover patterns.

Conclusions

The results obtained by these investigations indicate that net radiation dominates the snowcover energy balance during seasonal ablation, with soil heat, turbulent, and advective fluxes each comprising a minor proportion of the net energy exchange. Land cover type exerts the strongest control on the snowcover energy exchange processes by decreasing the solar radiation at the snow surface, enhancing thermal radiation, and decreasing the snowcover albedo through the deposition of fine organic debris. These canopy effects result in higher rates of meltwater release to soils beneath the deciduous canopy, relative to the mixed and conifer canopies. The deeper snowpack beneath the OA canopy extends the period of melt, such that complete snowcover ablation and soil warming begins at approximately the same time as beneath the OJP canopy. Although melt at the NSA sites began at the same time as the SSA sites, slower melt rates and deeper snowcovers beneath some canopies delayed complete meltout from approximately 4 to 14 days after the SSA sites. Between site analyses of simulated snowcover processes indicate that potential changes in both land cover and climate must be considered for investigations concerning responses of the boreal ecosystem to altered climate conditions.

The modeling results indicate that where high-quality below-canopy radiation data exist, simple canopy adjustment algorithms can be developed and applied to open site meteorological data to drive snowcover energy balance models. These results also demonstrate the effectiveness of the algorithms within a wide variety of canopy types, ranging from the highly transmissive OA canopy to the optically dense OBS canopy, by accurately representing snowpack deposition, and both the timing and rate of seasonal melt. The relative simplicity of the algorithms suggests that these techniques should be effective for distributed snowcover modeling. The canopy adjustments do not explicitly consider individual canopy elements, and may not be as effective for other land covers with significantly different structures. Canopy adjustment algorithms for rigorous spatially distributed snowcover simulations should therefore contain parameterizations

for tree species, height, dimension, and stem density relationships, while operating within a framework of commonly available spatial data products.

Bibliography

Berris, S. N., and R. D. Harr, Comparative snow accumulation and melt during rainfall in forested and clear-cut plots in the western Cascades of Oregon, *Water Resour. Res., 23*, 135-142, 1987.

Bonan, G. B., D. Pollard, and S. L. Thompson, Effects of boreal forest vegetation on global climate, *Nature*, 359, 716-718, 1992.

BOREAS Experiment Plan, *Boreal Ecosystem-Atmosphere Study Experiment Plan*, (ed. by P. Sellers, F. Hall, D. Baldocchi, J. Cihlar, P. Crill, J. Den Hartog, B. Goodison, R. Kelly, D. Lettenmeier, H. Margolis, J. Ranson, and M. Ryan), Version 3.1, May 1995.

Brutsaert, W., *Evaporation Into the Atmosphere*, 299 pp., D. Reidel, Hongham, Mass., 1982.

Colbeck, S. C., E. A. Anderson, V. C. Bissel, A. G. Crook, D. H. Male, C. W. Slaughter, and D. R. Wiesnet, Snow accumulation, distribution, melt, and runoff, *EOS Trans. AGU*, 60, 465-474, 1979.

Davis, R. E., J. P. Hardy, W. Ni, C. Woodcock, J. C. McKenzie. R. Jordan, and X. Li, Variation of snow cover ablation in the boreal forest: A sensitivity study on the effects of conifer canopy, *J. Geophys. Res.*, 102, 29389-29395, 1997.

Garen, D. C. and D. Marks, Spatially distributed snow modeling in mountainous regions - Boise River application, Proc. International Conference on Application of GIS in Hydrology and Water Resources Management, *IAHS Pub. No. 235*, 421-428, 1996.

Golding, D. L. and R. H. Swanson, Snow distribution patterns in clearings and adjacent forest, *Water Resour. Res.*, 22, 1931-1942, 1986.

Hardy, J. P., R. E. Davis, R. Jordan, X. Li, C. Woodcock, W. Ni, and J. C. McKenzie, Snow ablation modeling at the stand scale in a boreal jack pine forest, *J. Geophys. Res.*, 102, 29397-29405, 1997.

Jones, H. G., *Plants and microclimate, 2nd Ed.*, 428 pp., Cambridge University Press, New York, 1992.

Jordan, R., *A one-dimensional temperature model for a snow cover: Technical documentation for SNTHERM.89*, 49 pp., Cold Regions Research and Engineering Laboratory Special Report 91-16, 1991.

Lafleur, P. M., and P. Adams, The effect of subarctic woodland vegetation on the radiation balance of a melting snow cover, *Arch. Met. Geoph. Biocl., Ser. A*, 34, 297-310, 1986.

Larsen, J. A, *The Boreal Ecosystem*, 500 pp., Academic Press, New York, 1980.

Lundberg, A., and S. Halldin, Evaporation of intercepted snow: Analysis of governing factors, *Water Resour. Res.*, 30, 2587-2598, 1994.

Male, D. H., and R. J. Granger, Snow surface energy exchange, *Water Resour. Res.*, 17, 609-627, 1981.

Marks, D., *Climate, energy exchange, and snowmelt in Emerald Lake Watershed, Sierra Nevada*, PhD Dissertation, 158 pp., University of California at Santa Barbara, 1988.

Marks, D., J. Dozier, and R. E. Davis, Climate and energy exchange at the snow surface in the alpine region of the Sierra Nevada, 1, Meteorological measurements and monitoring, *Water Resour. Res.*, 28, 3029-3042, 1992.

Marks, D., and J. Dozier, Climate and energy exchange at the snow surface in the alpine region of the Sierra Nevada, 2, Snow cover energy balance, *Water Resour. Res.*, 28, 3043-3054, 1992.

Marks, D., J. Kimball, D. Tingey, and T. Link. The sensitivity of snowmelt processes to climate conditions and forest cover during rain-on-snow: A case study of the 1996 Pacific Northwest flood, *Hyd. Proc.*, in press.

Marks, D., J. Domingo, and J. Frew. Software tools for hydro-climatic modeling and analysis: Image Processing Workbench, USGS Version 2.0, Electronic Document **http://quercus.ars.pn.usbr.gov/~ipw**, *Open File Report* (in review), U.S. Agricultural Research Service, 1998.

Marshall, S. E., and S. G. Warren, Parameterization of snow albedo for climate models, in: Large scale effects of seasonal snow cover, B. E. Goodison, R.G. Barry, and J. Dozier, eds., *IAHS-AIHS Publication 166*, International Association of Hydrologic Sciences, Wallingford, U. K., 44-50, 1987.

Meng, F. R., C. P. A. Borque, K. Jewett, D. Daugharty, P. A. Arp, The Nashwaak experimental watershed project: Analysing effects of clearcutting on soil temperature, soil moisture, snowpack, snowmelt and stream flow, *Wat. Air Soil Poll.*, 82, 363-374, 1995.

Monteith, J. L., and M. H. Unsworth, *Principles of Environmental Physics, 2nd Ed.*, 291 pp., Edward Arnold, New York, 1990.

Ni, W., X. Li, C. E. Woodcock, J. L. Roujean, and R. E. Davis, Transmission of solar radiation in boreal conifer forests: Measurement and models, *J. Geophys. Res.*, 102, 29555-29566, 1997.

Ohta, T., T. Hashimoto, and H. Ishibashi, Energy budget comparison of snowmelt rates in a deciduous forest and an open site, *Ann. Glac.*, 18, 53-59, 1993.

Peixoto, J. P., and A. H. Oort, *Physics of Climate*, 520 pp., American Institute of Physics, New York. 1992.

Pomeroy, J. W. and Dion, K., Winter radiation extinction and reflection in a boreal pine canopy: Measurements and modelling, *Hyd. Proc.*, 10, 1591-1608, 1996.

Price, A. G., and D. E. Petzold, Surface Emissivities in a Boreal Forest During Snowmelt, *Arct. Alp. Res.*, 16, 45-51, 1984.

Price, M. A., A simplified scalable shading model for radiation at the forest floor, M.S. thesis, 43 pp., Dept. of Math., Oregon State Univ., 1997.

Risley, J., D. Marks, and T. E. Link, Application of a quasi-energy balance model to simulate snowmelt under variable canopies during a major rain-on-snow event, *EOS Trans. AGU, 78*, 258, 1997.

Schlesinger, M. E. and Mitchell, J. F. B., Climate model calculations of the equilibrium climatic response to increased carbon dioxide, *Rev. Geophys.*, 25, 760-798, 1987.

Schmidt, R. A., and D. R. Gluns, Snowfall interception on branches of three conifer species, *Can. J. For. Res.*, 21, 1262-1269, 1991.

Sellers, P. J., R. E. Dickinson, D. A. Randall, A. K. Betts, F. G. Hall, J. A. Berry, G. J. Collatz, A. S. Denning, H. A. Mooney, C. A. Nobre, N. Sato, C. B. Field, and A. Henderson-Sellers, Modeling the exchanges of energy, water, and carbon between continents and the atmosphere, *Science*, 275, 502-509, 1997.

Sellers, P., F. Hall, H. Margolis, B. Kelly, D. Baldocchi, G. den Hartog, J. Cihlar, M. G. Ryan, B. Goodison, P. Crill, K. J. Ranson, D. Lettenmaier, and D. E. Wickland, The Boreal Ecosystem-Atmosphere Study (BOREAS): An overview and early results from the 1994 field year, *Bull. Amer. Meteorol. Soc., 76*, 1549-1577, 1995.

Shewchuk, S. R., Surface mesonet for BOREAS, *J. Geophys. Res.*, 102, 29077-29082, 1997.

Shook, K., and D. M. Gray, Snowmelt resulting from advection, *Hyd. Proc.*, 11, 1725-1736, 1997.

Stegman, S.V., Snowpack changes resulting from timber harvest: Interception, redistribution, and evaporation, *Wat. Res. Bull.*, 32, 1353-1360, 1996.

Sturm, M., Snow distribution and heat flow in the taiga, *Arc. and Alp. Res.*, 24, 145-152, 1992.

Susong, D., D. Marks, D. Garen, and J. Mason, Application of an energy balance snowmelt model to estimate ground-water recharge in a mountain basin under varying climate conditions, *EOS Trans. AGU*, 77, 176, 1996.

Tans, P. P., Fung, I. Y., and Takahashi, 1990, Observational constraints on the global atmospheric CO_2 budget, *Science*, 247, 1431-1438, 1990.

Troendle, C. A., and R. M. King, The effect of timber harvest on the Fool Creek Watershed, 30 years later, *Water Resour, Res.*, 21, 1915-1922, 1985.

Warren, S. G., and W. J. Wiscombe, A model for the spectral albedo of snow. II. Snow containing atmosperic aerosols, *J. Atmos. Sci.*, 37, 2734-2745, 1980.

Wiscombe, W. J., and S. G. Warren, A model for the spectral albedo of snow. I. Pure snow, *J. Atmos. Sci.*, 37, 2712-2733, 1980.